COO-2262-10
MITNE-210

SPATIAL HOMOGENIZATION OF DIFFUSION THEORY PARAMETERS

by

B. A. Worley
A. F. Henry

September 1977

DEPARTMENT OF NUCLEAR ENGINEERING
MASSACHUSETTS INSTITUTE OF TECHNOLOGY
Cambridge, Massachusetts

ERDA Research and Development
Contract EY-76-S-02-2262
U. S. Energy Research and Development Administration

Massachusetts Institute of Technology
Department of Nuclear Engineering
Cambridge, Massachusetts

SPATIAL HOMOGENIZATION OF DIFFUSION THEORY PARAMETERS

by

B. A. Worley
A. F. Henry

September 1977

COO-2262-10

MITNE-210

ERDA Research and Development

Contract EY-76-S-02-2262

U. S. Energy Research and Development Administration

SPATIAL HOMOGENIZATION OF DIFFUSION THEORY PARAMETERS

by

BRIAN ADDISON WORLEY

Submitted to the Department of Nuclear Engineering
on August 12, 1977 in partial fulfillment of the requirements
for the Degree of Doctor of Philosophy

ABSTRACT

The use of Response Matrix Technique for finding two-group, two-dimensional equivalent diffusion theory parameters is proposed. A homogenization scheme for calculating assembly-constant group diffusion parameters which are dependent upon assembly position within the reactor results. Equivalent group diffusion parameters are determined by this response matrix scheme for assemblies typical of both BWR and PWR geometries. Their use in reactor criticality problems leads to an accurate prediction of assembly powers and reactor K_{eff}. The superiority of the group diffusion parameters found using the present scheme over the conventional flux-weighted constants is demonstrated.

Thesis Supervisor: Allan F. Henry

Title: Professor of Nuclear Engineering

ACKNOWLEDGEMENTS

I would like to express my sincere appreciation to Professor Allan F. Henry who served as thesis supervisor. Throughout the thesis work he was always willing to extend his professional insight as well as his friendship. His guidance in tackling various problems was concise and practical; his manner of explanation inspirational. I would like to thank him for his personal friendship both in good times and difficult ones.

Thanks are also extended to Professor Kent Hansen, who served as thesis reader.

Partial financial support was provided by the Energy Research and Development Administration.

This thesis was typed by Kris Hunter and I thank her for both her skill and patience.

Finally, I wish to extend my thanks to my family and friends for their support and friendship during the work of the past few years. I am particularly thankful for my close acquaintances in Brookline and for the warmth they have shown me during the last few months. I am most grateful to the Gauger family for all the happiness they have brought me. And I owe more than I can ever repay to Angie and Tom Markert for their guidance, friendship, and moral support. They have proved to be the best of friends during the most difficult of times. But more than anyone,

I would like to thank my parents for their continual love and guidance, and to them I dedicate this thesis.

TABLE OF CONTENTS

LIST OF FIGURES

LIST OF TABLES

CHAPTER I

Equivalent Diffusion Theory Parameters

1.1 Introduction

Analysis of the free-neutron behavior in a reactor requires the ability to predict the neutron density in space, direction, and energy. Transport theory methods such as a high order, multigroup, discrete ordinate approximation or Monte Carlo analysis[1] are capable of solving such complex problems but are prohibitively expensive for most practical reactor geometries. An alternative approach is to use group diffusion theory provided that the approximations made in going from the neutron transport equation to the neutron diffusion equation apply to the particular problem being solved.

The principal approximation required to obtain diffusion theory is that the neutron density in phase space, $N(\underline{r},\underline{\Omega},E)$, is represented by

$$N(\underline{r},\underline{\Omega},E) = F(\underline{r},E) + \underline{\Omega}\cdot\underline{V}(\underline{r},E) \quad , \tag{1.1}$$

where $F(\underline{r},E)$ and $\underline{V}(\underline{r},E)$ are a scalar and vector function of position and energy. This linearly anisotropic distribution can describe a general drift of neutrons but cannot even approximate a beam-like flow of neutrons[2]. Near physical boundaries where strong neutron absorbers may be adjacent to

highly scattering but weakly absorbing material, the direction of neutron flow will be strongly towards the absorbing material, and the use of diffusion theory will predict inadequately the neutron density. A light water reactor, for example, may contain small cylindrical fuel rods, lumps of burnable poison and control rods near which the neutron behavior tends to be highly directional so that the use of diffusion theory will lead to inaccurate results.

In order to predict, without solving the transport problem, the behavior of neutrons in a reactor consisting of assemblies which have all the aforementioned heterogeneities, certain techniques for finding regional, group "equivalent" cross sections and diffusion coefficients have been developed. These equivalent diffusion theory parameters are calculated in a two-step homogenization procedure. The first step determines equivalent diffusion parameters which are capable of describing the neutron behavior in a small region where the neutron currents tend to be hightly directional for particular energy ranges. Such regions occur in a fuel rod and the surrounding clad and moderator and near localized absorbers and control rods. Fortunately, the fuel cells (fuel, clad, and surrounding moderator) of each assembly, although many in number, are usually identical (at least at beginning of life) and prescriptions[3,4] have been developed which are capable of determining equivalent group diffusion constants for the cell which adequately describe

the cell-integrated reaction rates that would be obtained using exact transport calculations. Likewise, methods such as blackness theory are capable of determining the equivalent diffusion constants for localized poisons and control rods[5]. Once each assembly is entirely described by material zones for which equivalent group diffusion constants have been calculated, the entire neutron behavior throughout the reactor can be predicted by diffusion theory.

The need for a second step of homogenization becomes apparent upon the realization that a typical reactor may contain as many as 160 assemblies and 225 fuel or control cells per assembly. Thus after equivalent diffusion constants have been determined throughout the reactor from the first step of homogenization, a full-core problem depicting the heterogeneities within each assembly(fuel cells, control rods, etc.) would have a minimum of 36,000 mesh points per energy group per axial mesh plane for the core alone. To avoid this prohibitive expense, a second stage of homogenization is carried out in which "nodes" (usually entire assemblies) of the reactor are homogenized. Group-equivalent diffusion parameters, constant over an entire node, are calculated, and methods such as nodal or finite element[6,7,8] are applied to the full-core problem. The nodal and finite element methods permit a large mesh spacing over regions of constant (or nearly constant) material composition. This second state of homogenization therefore permits a full-core

solution to the group diffusion equations with a reasonable number of mesh points. It is this second state of homogenization which is the subject of the present thesis.

1.2 Spatially-Homogenized Diffusion Parameters

Once equivalent diffusion parameters have been found for small regions about any space point $\underline{r}$ from the first stage of homogenization, diffusion theory is applicable throughout the reactor core. The group diffusion equation in matrix form as derived from the P-1 approximation to the transport equation [2] is

$$-\nabla\cdot[\underline{J}(\underline{r})]-[A(\underline{r})][\phi(\underline{r})]+\frac{1}{\lambda}[M(\underline{r})][\phi(\underline{r})]=0 \qquad (1.2)$$

where

$$-\nabla\cdot[\underline{J}(\underline{r})]=\sum_u \frac{\partial}{\partial u}[D_u(\underline{r})]\frac{\partial}{\partial u}[\phi(\underline{r})] \quad ,$$

and the matrix elements are given by

$$[\phi(\underline{r})]=\text{Col}\{\phi_1(\underline{r}),\phi_2(\underline{r}),\ldots,\phi_G(\underline{r})\} \quad ;$$

$$[\underline{J}_x(\underline{r})]=[J_x(\underline{r})]\underline{i}$$

$$[\underline{J}_y(\underline{r})]=[J_y(\underline{r})]\underline{j}$$

$$[\underline{J}_z(\underline{r})] = [J_z(\underline{r})]\underline{k}$$

where

$$[J_u(\underline{r})] = \text{Col}\,\{J_{1u}(\underline{r}),\ J_{2u}(\underline{r}),\ldots,\ J_{Gu}(\underline{r})\}$$

$$u=x,y,z\ ;$$

$$[A(\underline{r})] \equiv \{A_{gg'}(\underline{r})\} \quad ,\ \text{a G x G matrix}$$

where

$$A_{gg'}(\underline{r}) \equiv \Sigma_{tg}(\underline{r})\delta_{gg'} - \Sigma_{gg'}(r) \quad ;$$

$$[M(\underline{r})] \equiv [\chi(r)][\nu\Sigma_f(\underline{r})] \quad ,\ \text{a G x G matrix}$$

where

$$[\chi(\underline{r})] = \text{Col}\,\{\chi_1,\ \chi_2,\ldots,\chi_G\}$$

and

$$[\nu\Sigma_f(\underline{r})] = \text{Col}\,\{\nu\Sigma_{f1}(\underline{r}),\nu\Sigma_{f2}(\underline{r}),\ldots,\nu\Sigma_{fG}(\underline{r})\} \quad .$$

Note that at each point $\underline{r}$ there will be only one set of equivalent diffusion parameters from the first step of homogenization.

The further homogenization over a large node of the reactor such as an assembly will yield a new set of cross sections denoted by $[\bar{D}_u]$, $[\bar{A}]$, and $[\bar{M}]$. This new set of parameters should have the following characteristics:

i) they should be constant over a given volume V_l;

ii) they are such that the eigenvalue $\bar{\lambda}$ determined from the equation

$$\sum_u \frac{\partial}{\partial u} [\bar{D}_u(\underline{r})] \frac{\partial}{\partial u} [\bar{\phi}(\underline{r})] - [\bar{A}(\underline{r})][\bar{\phi}(\underline{r})] + \frac{1}{\bar{\lambda}} [\bar{M}(\underline{r})][\bar{\phi}(\underline{r})] = 0$$

($\bar{\phi}(\underline{r})$ is solution using $[\bar{A}]$, $[\bar{M}]$, $[\bar{D}_u]$) is identical with that given by the solution of Eq. (1.2);

iii) they are such that the integrated reaction rates over each different V_l for each energy group are the same as those found by the solution of Eq. (1.2).

These conditions will be met if for each volume element V_1:

$$-\int_{V_i} \frac{\partial}{\partial u}[\underline{J}_u(\underline{r})]dV = [\bar{D}_u]_i \int_{V_i} \frac{\partial^2}{\partial u^2}[\bar{\phi}(\underline{r})]dV \ ,$$

$$\int_{V_i} [A(\underline{r})][\phi(\underline{r})]dV = [\bar{A}]_i \int_{V_i} [\bar{\phi}(\underline{r})]dV \ ,$$

$$\int_{V_i} [M(\underline{r})][\phi(\underline{r})]dV = [\bar{M}]_i \int_{V_I} [\bar{\phi}(\underline{r})]dV \ .$$

Since the $[\bar{D}_u]_i$, $[\bar{A}]_i$, and $[\bar{M}]_i$ can be full G x G matricies (the $\bar{D}_{gg'}$ elements for $g \neq g'$ exist for particular derivations of the diffusion coefficients from the P-1 equation; see reference (2)) and since each therefore contains G^2 unknown terms, determination of each element of $[\bar{D}_u]_i$, $[\bar{A}]_i$, or $[\bar{M}]_i$ would require G^2 equations. The above three matrix equations each result in only G equations. Therefore the elements of $[\bar{D}_u]_i$, $[\bar{A}]_i$, and $[\bar{M}]_i$ are found by requiring a term by term equivalence of each integral. For example,

it is required that

$$\int_{V_i} A_{gg'}(\underline{r})\phi_{g'}(\underline{r})\,dV = \bar{A}^{i}_{gg'} \int_{V_i} \bar{\phi}_{g'}(\underline{r})\,dV$$

$$(g=1,2,\ldots,G;\ g'=1,2,\ldots,G).$$

Thus each term of $[\bar{D}_u]$, $[\bar{M}]$, and $[\bar{A}]$ can be found once

$\int_{V_i} [\bar{\phi}(\underline{r})]\,dV$ and $\int_{V_I} \frac{\partial^2}{\partial u^2} [\bar{\phi}(\underline{r})]\,dV$ are known.

Specifically, the "ideal" equivalent cross section for interaction α, group g, $\bar{\Sigma}^{(i)}_{\alpha g}$, and the group diffusion coefficient for direction u (for most derivations $[\bar{D}_u]$ is a diagonal matrix), $\bar{D}^{(i)}_{gu}$, then obey

$$\bar{\Sigma}^{(i)}_{\alpha g} = \frac{\int_{V_i} \Sigma_{\alpha g}(\underline{r})\phi_g(\underline{r})\,dV}{\int_{V_i} \bar{\phi}_g(\underline{r})\,dV} \tag{1.3}$$

and

$$\bar{D}^{(i)}_{g,u} = -\frac{\int_{V_i} \frac{\partial}{\partial u} J_{gu}(\underline{r})\,dV}{\int_{V_i} \frac{\partial^2}{\partial u^2} \bar{\phi}_g(\underline{r})\,dV} \tag{1.4}$$

where $\phi_g^{(i)}(\underline{r})$ and $\Sigma_{\alpha g}^{(i)}(\underline{r})$ are the group g flux and interaction cross section for process α, node i in the heterogeneous reactor and $\bar{\phi}_g^{(i)}(\underline{r})$ and $\bar{\Sigma}_{\alpha g}^{(i)}$ are the corresponding quantities when node i is homogenized.

Equivalent group diffusion constants, constant over node i, can be calculated by Eqs. (1.3) and (1.4). However, their calculation requires an apriori knowledge of the integrated reaction rate and leakage rate out of node i in the heterogeneous reactor. Moreover, even if a knowledge of these quantities is assumed, the flux shape resulting from the use of the homogenized constants, $\bar{\phi}_g(\underline{r})$, is required. This situation introduces a nonlinearity into the calculation of the equivalent constants, and, since $\bar{\phi}_g(\underline{r})$ is constricted to be a solution of the diffusion equation, it may in fact negate the existence of such constants.

1.3 Flux-Weighted Constants (FWC)

The most common method of calculating equivalent diffusion constants for a given node i is to relax the conditions that the $\bar{\Sigma}_{\alpha g}^{(i)}$ and $\bar{D}_{gu}^{(i)}$ defined by Eqs. (1.3) and (1.4) must obey. In the usual flux-weighting procedure, the equivalent cross sections are calculated under the assumption that

$$\int_{V_i} \bar{\phi}_g(\underline{r})\,dV = \int_{V_i} \phi_g(\underline{r})\,dV \quad .$$

However, it is unlikely that the integrated flux in node i in the reactor consisting of homogenized assemblies will equal the corresponding integrated flux in node i of the heterogeneous reactor. This is the first serious theoretical weakness encountered when using FWC.

A second fundamental weakness resulting from using FWC is that the homogenized diffusion coefficients are usually defined such that

$$\frac{1}{\bar{D}_{gu}^{(i)}} = \frac{\int_{V_i} \frac{1}{D_{gu}^{(\underline{r})}} \phi_g(\underline{r}) dV}{\int_{V_i} \phi_g(\underline{r}) dV} \qquad (1.5)$$

The justification for calculating $\bar{D}_{gu}^{(i)}$ by Eq. (1.5) is that $\frac{1}{D_{gu}^{(\underline{r})}} \simeq \Sigma_{g,\text{transport}}(\underline{r})$ and Eq. (1.5) leads to a conservation of the transport rate. This reasoning is invalid, however, since the transport cross section defined by the P-1 approximation to the transport equation is a function of the neutron current, and weighting by the neutron flux preserves no integrated reaction rate.

A final important point is one concerning the calculation of the integrated flux shape of the heterogeneous reactor,

$\phi_g(\underline{r})$, within each node i. This shape is needed in the calculations of the homogenized cross sections and diffusion coefficients as defined in Eqs. (1.3) and (1.5). The flux shape for the heterogeneous node i is determined by isolating the node in question and solving the group-diffusion eigenvalue problem under the assumption that the net leakage out of each side of the node is zero. The justification for this approximation is that most nodes (assemblies) in a reactor are surrounded by assemblies of nearly the same composition and that the global flux shape across most assemblies (with the exception of those near the reflector) will have only a slight overall curvature. For a situation such as this, the net leakage across each face of the node will be small. Nevertheless, the zero current boundary condition assumption is not exact and is even inaccurate for assemblies near the reflector or for any other reactor condition where significant flux-tilting may occur.

Summarizing: Flux-weighted constants (FWC) are determined by a set of calculations in which three plausible assumptions are made:

$$(1) \quad \int_{V_i} \bar{\phi}_g(r)\,dV = \int_{V_i} \phi_g(r)\,dV \quad ,$$

$$(2) \qquad \frac{1}{\overline{D}_{gu}(r)} = \frac{\int \frac{1}{D_{gu}(r)} \phi_g(\underline{r}) dV}{\int \phi_g(\underline{r}) dV} \quad ,$$

(3) all assemblies are assumed to have negligible net leakage across each face, regardless of the assembly position in the reactor.

1.4 Equivalent Group Diffusion Coefficients (EGDC)

The theoretical inconsistencies inherent in the calculation of FWC as described in the previous section suggest that a more exact set of equivalent group diffusion parameters may be determined if the weaknesses in the flux-weighting procedure are avoided or if an entirely different approach to homogenization can be found which circumvents these weaknesses. Earlier work gives evidence that an improved spatial-homogenization technique can be found.

For one-dimensional reactor geometries, Kollas[9] has shown that one and two-group EGDC can be found which are "exact" (i.e. their use will reproduce exactly the integrated reaction rates and leakage rates in each assembly as determined by a heterogeneous, full-core calculation) for reactors in which the material in each slab assembly comprising the reactor is located symmetrically about the

center plane of the assembly. This homogeneous procedure involves a calculation of the EGDC by matrix manipulation. It is dissimiliar to any flux-weighting procedure and yields homogenized parameters different from the usual flux-weighted quantities.

For two-dimensional reactor geometries and two energy groups, previous work [10] has provided a means for calculating EGDC from a flux-weighting standpoint, but using a Response Matrix [11,12] approach. This procedure has the flavor of Kollas's technique in one dimension, and reduces to the exact answer for one-dimensional, one-group problems. The major theoretical improvements in this response matrix approach for calculating 2-D, 2-group EGDC is that the $\int_{V_i} \bar{\phi}_g(\underline{r})\,dV$ appearing in Eq. (1.1) are determined in a more exact manner. (It is no longer assumed that $\int_{V_i} \bar{\phi}_g(\underline{r})\,dV = \int_{V_i} \phi_g(\underline{r})\,dV$ as is done in calculating FWC.) Secondly, the homogeneous diffusion coefficients for assembly i are determined by trying to reproduce as closely as possible the exact transmission of neutrons that occur in assembly i in the heterogeneous reactor. This criteria, although vague in definition, provides a much stronger physical foundation for determining the homogenized diffusion coefficients than does the use of Eq. (1.5). Finally, the zero current boundary conditions along each face

of the assembly being homogenized is replaced by a more realistic boundary condition which allows a net leakage across each face of the assembly.

The purpose of this thesis is to examine this response matrix approach for calculating two-dimensional, two-group equivalent group diffusion constants. In particular, efforts are directed towards (1) decreasing the amount of computational effort required in calculating the EGDC and (2) improving the methodology of the homogenization technique such that a further increase in accuracy is provided by the use of the resulting EGDC.

In Chapter 2 we review the response matrix technique in general and its application in finding 2-D, 2-group EGDC. We then examine resulting strengths and weaknesses of the EGDC as indicated by their use in a typical light-water reactor problem. In Chapter 3 we present a technique for improving upon the weaknesses of the present response matrix scheme, and in Chapter 4 we present results of the use of these EGDC for BWR and PWR reactor geometries. Chapter 5 contains the conclusions of this work and recommendations for further study.

CHAPTER II

DETERMINATION OF TWO-DIMENSIONAL, TWO-GROUP EGDC USING A RESPONSE MATRIX SCHEME

2.1 The Response Matrix Technique in Two Dimensions

The response matrix method consists of replacing a region of a reactor, usually an assembly, by a black box connected with the rest of the reactor by response matrices. In practice the entire reactor is divided into black boxes which are interconnected with adjacent boxes by precalculated response matrices. A reactor criticality calculation involving these matrices gives the distribution of the partial neutron currents along the boundaries of each box. The partial currents are then used to calculate integrated reaction rates and to calculate the flux at any point in the reactor.

The calculation of the distribution of the partial currents requires a knowledge of these currents at each point along the boundaries of the assemblies and the resulting number of unknown parameters is infinite. Therefore, a particular spatial shape is assumed for the partial currents beforehand. For two-dimensional reactor configurations, the choices of both flat shapes and linear shapes have been examined with fairly successful results[11,12].

In applying the response matrix technique, the linear nature of the group diffusion equations is used in order to apply the principle of superposition. The incoming partial current along one side of an assemlby gives rise to outgoing

partial currents along all four sides of the assembly. By the principle of superposition, the total outgoing partial current on each face of the assembly is the sum of the contributions from each incoming current. The response matrices provide the various relationships between the incoming and outgoing partial currents of the four edges of an assembly. These response matrices therefore depend upon the distribution of incoming and outgoing partial currents along each face as well as the assembly composition. Accordingly, the flat or linear shape assumed for the aforementioned criticality calculation is also used as the distribution of the incoming currents to calculate the response matrices. For the purpose of using response matrices to calculate homogenized cross sections, the incoming group partial currents will be assumed to be spatially flat.

The response matrices which are used in the reactor criticality calculation are determined by a separate calculation for each assembly. Fortunately, most reactors have only three or four different assembly compositions at beginning of life. In order to calculate the response matrices for a given assembly composition, the assembly is isolated in a vacuum and the group g (g=1,2,...,G) partial current leaving each face is calculated for a spatially flat, unit incoming group g' (g'=1,2,...,G) partial current. The integrated partial currents along each face are then related by the response matrices. With a spatially flat, unit incoming

partial current assumed, the response matrix elements are actually the fraction of the integrated group g' (g'=1,2,...,G) partial current incident upon face ℓ' which appears in the energy group g (g=1,2,...,G) and leaves face ℓ. Symbolically, each response matrix element can be represented by $R^{\ell\ell'}_{gg'}$, where

$$R^{\ell\ell'}_{gg'} = \text{the fraction of the integrated group g' (g'=1,2,...,G) partial current incident upon face } \ell' \text{ which appears in energy group g (g=1,2,...G) and leaves face } \ell. \qquad (2.1)$$

Another quantity which can be determined during the calculation of the response matrices is the assembly-integrated reaction rate of process α for neutrons appearing in group g. A corresponding integrated reaction rate response matrix element, denoted by $I^{\ell'}_{gg'}(\alpha)$, is defined such that

$$I^{\ell'}_{gg'}(\alpha) = \text{the assembly-integrated reaction rate of process } \alpha \text{ for neutrons appearing in group g as a result of a spatially flat, unit incoming current in group g', along face } \ell'. \qquad (2.2)$$

Once the actual incoming partial currents along each face of the assembly are known, Eqs. (2.1) and (2.2) can be used to calculate the total outgoing partial currents along each face as well as the integrated group reaction rates. Specifically, the outgoing partial current in group g along face ℓ, denoted by $J_g^{\ell}(\text{out})$ can be determined by

$$J_g^{\ell}(\text{out}) = \sum_{\ell'=1}^{4} \sum_{g'=1}^{G} R_{gg'}^{\ell\ell'} J_{g'}^{\ell'}(\text{in}) \qquad (2.3)$$

where $J_{g'}^{\ell'}(\text{in})$ is the incoming group g' partial current along face ℓ'. Likewise, the integrated reaction rate for process α, group g is denoted by $I_g(\alpha)$ and is calculated by

$$I_g(\alpha) = \sum_{\ell'=1}^{4} \sum_{g'=1}^{G} I_{gg'}^{\ell'}(\alpha) J_{g'}^{\ell'}(\text{in}). \qquad (2.4)$$

The application of the response matrix technique to the determination of equivalent group diffusion constants is confined to the step in which the response matrices for each assembly composition are calculated. This step will hereafter be refered to as the cell calculation. The reactor

criticality equation using these response matrices comprises the second stage of calculation of the response matrix technique and is not used during the assembly-homogenization procedure.

In the next section a successful method for calculating two-dimensional, two-group diffusion theory constants based upon the determination of response matrices is outlined. Results of this method and ideas for improvement are discussed in the last two sections of this chapter.

2.2 A Spatial Homogenization Scheme Based Upon a Response Matrix Approach

The theoretical weaknesses of the conventional flux-weighting procedure for finding assembly-constant, equivalent group diffusion parameters (denoted by FWC) are discussed in Chapter I. Although Kollas[9] has shown that an alternative approach of calculating equivalent diffusion constants for certain slab geometries circumvents these weaknesses, his scheme cannot be extended to the two-dimensional problem. A method for calculating two-dimensional, two-group equivalent diffusion constants has been developed previously[10] which uses a response matrix approach in order to improve upon the aforementioned weaknesses of the conventional flux-weighting procedure. The equivalent group diffusion constants (EGDC) determined by this technique are different than the corresponding FWC; and, the use of the EGDC in a full-core problem

provides a better prediction of the assembly-integrated power density and core eigenvalue than does the use of FWC. The methodology of this previous response matrix approach for determining EGDC will be discussed in order to examine its relative strengths and weaknesses.

The equivalent cross section for process α, group g is defined in Eq. (1.3). An equivalent definition in terms of integrated reaction rate responses is given by

$$\bar{\Sigma}^{(i)}_{\alpha g} = \frac{\sum_{\ell'=1}^{4} \sum_{g'=1}^{G} I^{\ell'}_{gg'}(\alpha,i) J^{\ell'}_{g'}(in,i)}{\sum_{\ell'=1}^{4} \sum_{g'=1}^{G} \bar{\phi}^{\ell'}_{gg'}(i)\, \bar{J}^{\ell'}_{g'}(in,i)} \qquad (2.5)$$

where $I^{\ell'}_{gg'}(\alpha,i)$ is the integrated reaction rate response in assembly i in the <u>heterogeneous</u> reactor; $J^{\ell'}_{g'}(in,i)$ is the group g' partial current entering face ℓ' of the node i in the <u>heterogeneous</u> reactor; $\bar{\phi}^{\ell'}_{gg'}(i)$ is the integrated group g flux response for an incoming unit partial current in group g' entering face ℓ' in assembly i in the <u>homogeneous</u> reactor; and $\bar{J}^{\ell'}_{g'}(in,i)$ is the group g' partial current entering face ℓ' of node i in the <u>homogeneous</u> reactor. A stronger condition is then imposed upon the calculation of

$\bar{\Sigma}_{\alpha g}^{(i)}$ from Eq. (2.5) by requiring that $\bar{J}_{g}^{\ell'}(in,i)=J_{g}^{\ell'}(in,i)$. Thus, $\bar{\Sigma}_{\alpha g}^{(i)}$ will be defined in terms of integrated response matrix as

$$\bar{\Sigma}_{\alpha g}^{(i)} \equiv \frac{\sum_{\ell'=1}^{4} \sum_{g'=1}^{G} I_{gg'}^{\ell'}(\alpha,i)\, J_{g'}^{\ell'}(in,i)}{\sum_{\ell'=1}^{4} \sum_{g'=1}^{G} \bar{\phi}_{gg'}^{\ell'}(i)\, J_{g'}^{\ell'}(in,i)} \qquad (2.6)$$

This definition of $\bar{\Sigma}_{\alpha g}^{(i)}$ is used in the previous response matrix approach and will also be used as a basis for calculating the $\bar{\Sigma}_{\alpha g}^{(i)}$'s in the improved response matrix scheme introduced in Chapter III.

The $I_{gg'}^{\ell'}(\alpha,i)$ are determined for the heterogeneous node in a straightforward fixed source calculation (the cell calculation) by imposing a group g' unit incoming partial current along face ℓ' and calculating the resulting integrated reaction rate for neutrons in group g undergoing interaction α. The values of $\bar{\phi}_{gg'}^{\ell'}(i)$ and $J_{g'}^{\ell'}(in,i)$, however, cannot be calculated in a straightforward manner. A knowledge of the $J_{g'}^{\ell'}(in,i)$'s requires a full-core heterogeneous solution to the group diffusion equation (a self-defeating process), and $\bar{\phi}_{gg'}^{\ell'}(i)$, the flux solution in the homogeneous reactor, must be determined in a non-linear fashion since the

equivalent cross sections used in the homogeneous reactor solution depend upon the $\bar{\phi}^{\ell'}_{gg'}(in)$'s. In order to calculate the $\bar{\phi}^{\ell'}_{gg'}(i)$ and $J^{\ell'}_{g'}(in,i)$ several assumptions are made.

The previous homogenization procedure using a response matrix approach was performed for assemblies which had material placed symmetrically about the centerpoint. For such symmetric assemblies which are themselves surrounded by a large number of like assemblies, one can assume that for each energy group g and each assembly i, the $J^{\ell'}_{g'}(in,i)$ for all ℓ' (ℓ'=1,2,3,4) are identical. In the previous approach no distinction was made for assembly location and all assemblies were assumed to be surrounded by like assemblies. For that case, $\bar{\Sigma}^{(i)}_{\alpha g}$ for a symmetric assembly is given by

$$\bar{\Sigma}^{(i)}_{\alpha g} = \frac{\sum_{g'=1}^{G} I^{1}_{gg'}(\alpha,i)\, J^{1}_{g'}(in,i)}{\sum_{g'=1}^{G} \bar{\phi}^{1}_{gg'}(i)\, J^{1}_{g'}(in,i)} \qquad (2.7)$$

for all i. Note that $I^{1}_{gg'}(\alpha,i)$ and $J^{1}_{g'}(in,i)$ are the integrated reaction response and incoming group g' partial current for neutrons entering face 1. Neutrons are arbitrarily chosen to be entering face 1 since the $J^{\ell'}_{g'}(in,i)$ are assumed equal for all ℓ' for a given g', and since the

$I^{\ell'}_{gg'}$, for a given g and g' are equal for all ℓ' because of the assembly symmetry. Thus, the $I^{1}_{gg'}(\alpha,i)$'s are calculated in a cell calculation that consists of determining response matrices for group partial currents incident upon only one face. This situation results in a sizable reduction in the amount of computation required.

For two energy groups, $\bar{\Sigma}^{(i)}_{\alpha g}$ obeys

$$\bar{\Sigma}^{(i)}_{\alpha g} = \frac{X\, I^{1}_{g1}(\alpha,i) + I^{1}_{g2}(\alpha,i)}{X\, \bar{\phi}^{1}_{g1}(i) + \bar{\phi}^{1}_{g2}(i)} \qquad (2.8)$$

where $X=J^{1}_{1}(in,i)/J^{1}_{2}(in,i)$, the ratio of the incoming group one partial current along face one to the incoming group two partial current along face one. If it is assumed that

$$J^{1}_{1}(in,i)/J^{1}_{2}(in,i) = \sum_{\ell'=1}^{4} J^{1}_{1}(out,i) \Big/ \sum_{\ell'=1}^{4} J^{1}_{2}(out,i), \text{ where}$$

$J^{\ell'}_{g}(out,i)$ is the group g outgoing partial current along face ℓ' resulting from the incoming partial currents $J^{1}_{1}(in,i)$ and $J^{1}_{2}(in,i)$, then one can show that

$$X = \frac{C_{11}-C_{22}+\sqrt{(C_{22}-C_{11})^2+4C_{12}C_{21}}}{2C_{21}} \qquad (2.9)$$

where

$$C_{gg'} \equiv \sum_{\ell'=1}^{4} R_{gg'}^{\ell'} \quad .$$

Once the value of $X(J_1^1(in,i)/J_2^1(in,i))$ is calculated from Eq. (2.9), the values of the $\bar{\phi}_{gg'}^{1}(\alpha,i)$ must be determined before $\bar{\Sigma}_{\alpha g}^{(i)}$ can be found from Eq. (2.8). This can be accomplished by an iterative scheme. First, all responses are determined for the heterogeneous assembly i. Then $\bar{D}_1^{(i)}$ and $\bar{D}_2^{(i)}$, the group one and group two diffusion coefficients for assembly i, are chosen (see below). As a first guess, the homogenized cross sections are calculated from Eq. (2.8) with $\bar{\phi}_{gg'}^{1}(i)=\phi_{gg'}^{1}(i)$. The diffusion coefficients are then used in conjunction with this first guess of the $\bar{\Sigma}_{\alpha g}^{(i)}$'s in a cell calculation for the now <u>homogeneous</u> assembly, and new values of $(X\bar{\phi}_{g1}^{1}(i)+\bar{\phi}_{g2}^{1}(i))$ are calculated for each group g using the same value of X that was used in the heterogeneous cell calculation. This revised estimate of $(X\bar{\phi}_{g1}^{1}(i)+\bar{\phi}_{g2}^{1}(i))$ $[\neq(X\phi_{g1}^{1}(i)+\phi_{g2}^{1}(i)]$ is used in Eq. (2.8)

and a new value of $\bar{\Sigma}_{\alpha g}^{(i)}$ is calculated. This iterative process is continued until the use of a set of $\bar{\Sigma}_{\alpha g}^{(i)}$'s in the cell calculation for assembly i will result in the same value of $X\bar{\phi}_{g1}^{-1}(i)+\bar{\phi}_{g2}^{-1}(i)$ for g=1,2 as that used in determining the $\bar{\Sigma}_{\alpha g}^{(i)}$'s from Eq. (2.8). Thus, if the incoming group partial currents along each face of assembly i used in the cell calculation (where here it was assumed that for each g' and i the $J_{g'}^{\ell'}(i)$ are equal for all ℓ' and that X is given by Eq. (2.9)) match the corresponding partial currents in the homogeneous full-core solution, then the use of the $\bar{\Sigma}_{\alpha g}^{(i)}$'s as determined from Eq. (2.8) will preserve the "true" integrated reaction rates in assembly i as calculated from the numerator of the ratio in Eq. (2.8).

The values of $\bar{D}_1^{(i)}$ and $\bar{D}_2^{(i)}$ are chosen such that the transmission of neutrons through the homogeneous assembly i will most closely match the corresponding transmission of neutrons through the heterogeneous assembly. This could best be done if a $\bar{D}_1^{(i)}$ and $\bar{D}_2^{(i)}$ could be found such that $\bar{R}_{gg'}^{\ell\ell'}(i)=R_{gg'}^{\ell\ell'}(i)$ for all g, g', ℓ, and ℓ'. However, being able to match the many response matrix elements, $R_{gg'}^{\ell\ell'}(i)$, with only two degrees of freedom, $\bar{D}_1^{(i)}$ and $\bar{D}_2^{(i)}$, is unlikely. In fact, the best procedure for determining a set of $\bar{D}_1^{(i)}$ and $\bar{D}_2^{(i)}$ is to match the largest value of $R_{gg}^{\ell 1}$ for each g as calculated from the heterogeneous cell calculation. This

requires a double search procedure. Thus, for fixed values of $\bar{\Sigma}_{\alpha g}^{(i)}$'s, $\bar{D}_1^{(i)}$ and $\bar{D}_2^{(i)}$, yielding homogeneous response elements matching the largest $R_{11}^{\ell 1}(i)$ and $R_{22}^{\ell 1}(i)$, are found. However, the $\bar{\Sigma}_{\alpha g}^{(i)}$'s themselves must then be calculated iteratively for the newly found fixed values of the homogenized group diffusion coefficients. Fortunately this double-iterative procedure converges quickly.

The procedure outlined in this section is the previously tested scheme. The purpose of reviewing the technique is to demonstrate a response matrix approach for calculating equivalent diffusion theory constants. In addition, specific areas for improvement become apparent. A major goal of the present thesis is to improve upon the weaknesses in the scheme just outlined.

2.3 Results

Before discussing the weaknesses of the above homogenization technique, the strengths of the response matrix approach for calculating EGDC should be mentioned. First, the group diffusion coefficients are obtained in a manner that accounts for the true transmission of neutrons through the cell. The normal flux-weighted values (Eq.(1.5)) are conceptually inferior in this regard. Second, the net group currents at the boundaries of the assembly being homogenized can have non-zero values. This non-zero boundary condition is not allowed in the normal flux-weighting

scheme in which a zero net current is assumed along each face of the assembly. Finally, the $\bar{\Sigma}_{\alpha g}^{(i)}$'s are calculated using a good prediction of $\int_{V_i} \bar{\phi}_g(\underline{r})dV$ required for Eq. (1.3). In the usual flux-weighting scheme $\int_{V_i} \bar{\phi}_g(\underline{r})dV$ is assumed equal to $\int_{V_i} \phi_g(\underline{r})dV$. Note that the ability to match the integrated reaction rates resulting from the homogeneous cell calculation to those of the heterogeneous cell calculation is important since the cell calculation approximately represents the actual environmental conditions which a given assembly will experience in the full-core problem.

The response matrix approach for calculating EGDC just described was used to find equivalent, two-group diffusion parameters for a reactor with assemblies typical of a boiling water reactor. Figure 2.1 shows the assembly geometries for the two types of assemblies in the reactor. Both assembly types have material placed symmetrically about the centerpoint. The cross-shaped figure in one assembly represents control rod material and the cross-shape of the other assembly represents water. A water reflector surrounds

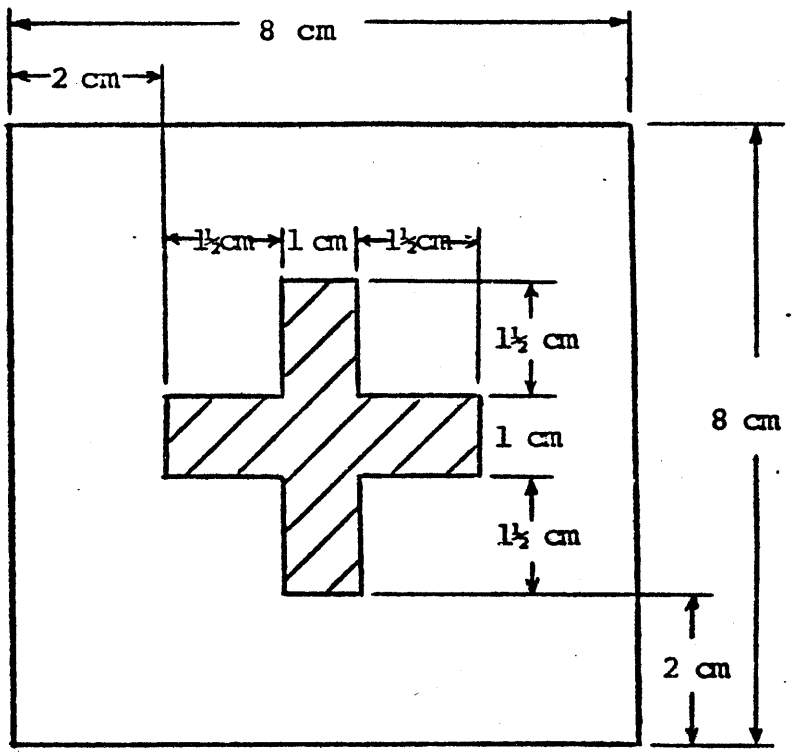

Two BWR assemblies have the above geometry but differ with respect to crossed-rod material.

	Crossed Rod
Assembly A	control rod material
Assembly B	water

FIGURE 2.1

BWR Assembly Compositions

TABLE 2.1

Diffusion Theory Parameters - FWC and EGDC

BWR Quarter-Core Problem with EGDC
Found From Previous R.M. Method

Assembly Type*	$\bar{D}_2$	$\bar{\Sigma}_{a1}$ / $\bar{\Sigma}_{a2}$	$\overline{\nu\Sigma}_{f1}$ / $\overline{\nu\Sigma}_{f2}$	$\bar{\Sigma}_{21}$ / --
EGDC				
Assembly A	1.4093+0	9.6928-3	6.4859-3	1.4194-2
	3.8073-1	1.0796-1	1.2549-1	---
Assembly B	1.4416+0	9.3719-3	6.4699-3	1.7231-2
	3.9246-1	9.6579-2	1.4333-1	---
FWC				
Assembly A	1.3884+0	9.7122-3	6.4987-3	1.4222-2
	3.8420-1	1.2155-1	1.4303-1	---
Assembly B	1.4470+0	9.4224-3	6.5050-3	1.7302-2
	3.7478-1	8.9222-2	1.3241-1	---

*Assembly type refers to Figure 2.1.

XX	Per cent error in power - FWC
XX	Per cent error in power - EGDC

1.74 -3.39	-3.88 1.01	3.67 -1.84
	5.63 - .01	-3.18 1.63
		5.81 .09

	FWC	EGDC
Per cent error in K_{eff}	-.847	-.890

FIGURE 2.2

BWR Quarter-Core Problem with EGDC Found From Previous Response Matrix Homogenization Scheme

the reactor core. EGDC and the conventional FWC were calculated for both assembly types and are listed in Table 2.1. A full-core criticality calculation was performed for the fine-mesh heterogeneous reactor geometry. Two full-core criticality calculations were then performed for the reactor consisting of homogenized assemblies with EGDC and FWC respectively. The resulting per cent errors in assembly powers and reactor K_{eff} are shown in Fig. 2.2 for the homogenized core solutions using the EGDC and the FWC. The use of EGDC shows a marked improvement over the use of FWC.

2.4 Ideas for Improving the Previous Response Matrix Approach for Calculating EGDC

Although the response matrix method just described results in equivalent diffusion constants that predict neutron behavior more accurately, there are several areas for improving the previous scheme. The first obvious weakness is that all assemblies are assumed to be part of a large number of like assemblies. In reality, however, many assemblies in a typical reactor are surrounded by similar, but not identical, types of assemblies. In addition, there are also a number of assemblies with at least one face adjacent to the reflector. Thus, one improvement upon the previous response matrix approach would be a method of estimating the $J_{g'}^{\ell'}(in,i)$'s needed in Eq. (2.5) which takes into account the location of the assembly in the reactor.

The other major weakness of the previous scheme is that the determination of the $\bar{\Sigma}_{\alpha g}^{(i)}$'s and $\bar{D}_{g}^{(i)}$'s requires a costly double-iterative scheme. An important improvement would be to reduce the amount of computational effort required in calculating the EGDC.

In the following chapter an alternative response matrix technique is presented that eliminates much of the computational effort required in the determination of the EGDC and also accounts for assembly position in the reactor.

CHAPTER III

AN IMPROVED RESPONSE MATRIX APPROACH FOR THE CALCULATION OF EGDC

3.1 Introduction

The response matrix approach for calculating homogenized group diffusion parameters leads to a set of EGDC which are an improvement on the conventional FWG as is evident from the results presented in Chapter 2. However, there are still areas for improvement over the previous scheme. Two specific improvements, which are discussed at the end of the preceding chapter, would be (1) a method of determining the incoming group partial currents along each edge of the assembly being homogenized (the $J_{g'}^{\ell'}$,(in,i)'s) that would reflect that particular assembly's position in the reactor; and (2) a technique for calculating the $\bar{\Sigma}_{\alpha g}^{(i)}$'s and $\bar{D}_{g}^{(i)}$'s that would require less computational effort than the previous double-iterative scheme.

In the next two sections of this chapter a method is presented which accomplishes the two aforementioned goals. The calculation of the equivalent group diffusion coefficients is discussed in Section 3.4.

3.2 A Homogenization Scheme Dependent Upon Assembly Location Within The Reactor

Equivalent group cross sections which are computed in terms of integrated reaction rate response matrices and

incoming group partial currents are defined in Eq. (2.6). In order to determine $\bar{\Sigma}_{\alpha g}^{(i)}$ using Eq. (2.6), values of the incoming group partial currents incident upon each face of the assembly, the $J_{g'}^{\ell'}(in,i)$'s, must be available. One approach is to assume that each assembly is surrounded by a large number of assemblies identical to the one being homogenized. For such assemblies, the incoming group g partial current will be the same along each of the four faces; and, for two energy groups, the calculation of $\bar{\Sigma}_{\alpha g}^{(i)}$ depends only upon the ratio of the incoming group partial currents (see Eq. (2.8)). A method for approximating this ratio is outlined in Chapter 2.

The previous scheme for determining EGDC makes the above assumption for each assembly in the reactor. Thus, the calculation of homogenized constants must be carried out only for each different assembly composition. However, the results shown in Figure 2.2 indicate that the per cent error in assembly power is highest for assemblies located at the core-reflector interface. The homogenization procedure is less accurate for these assemblies since the above semi-infinite-medium assumptions are not valid near the core surface.

A homogenization method is now presented in which the position of each assembly is considered in order to calculate the $J_{g'}^{\ell'}(in,i)$'s needed in Eq. (2.6). Although a different set of cross sections are calculated for each assembly position,

the same technique is used to determine all cross sections, and the same scheme is used to determine the $J_{g'}^{\ell'}(in,i)$'s for each position. The extra cost needed to account for an assembly position is small in comparison to the total cost of first finding equivalent constants and then solving the resultant full-core problem, and the increase in accuracy seems warranted.

The first stage of the present method is to calculate the response matrices for each different assembly composition. (Here the reference to a particular assembly composition includes its geometry.) For assemblies with quarter-assembly symmetry, only the response matrices for neutrons incident upon one face are determined. The spatial shape of the incoming group partial currents is assumed to be flat. The outgoing group partial current shape is then taken as that shape resulting from the cell calculation. (Recall that the cell calculation is the fixed-source calculation in which an integrated, unit group partial current incident upon a particular face gives rise to group flux shapes throughout the assembly. The calculation is performed for an incident partial current of each group ($g'=1,2,\ldots,G$.) A pictoral representation of the cell calculation for two energy groups and for a quarter-symmetric assembly is shown in Figure 3.1.

In order to determine the equivalent group cross sections using Eq. (2.6), the actual value of each of the

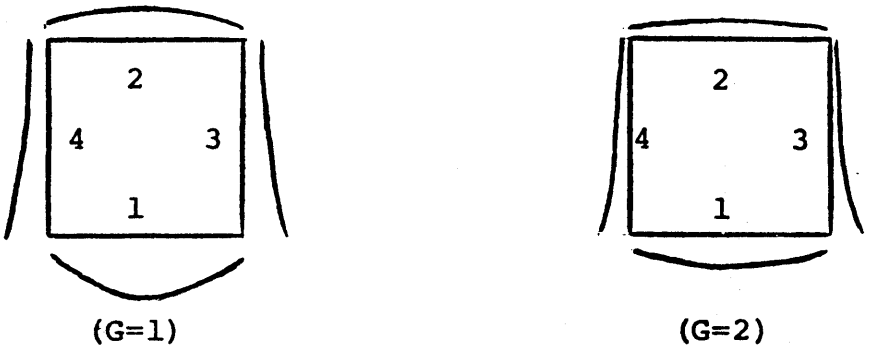

Incoming Group One Partial Current (G'=1)

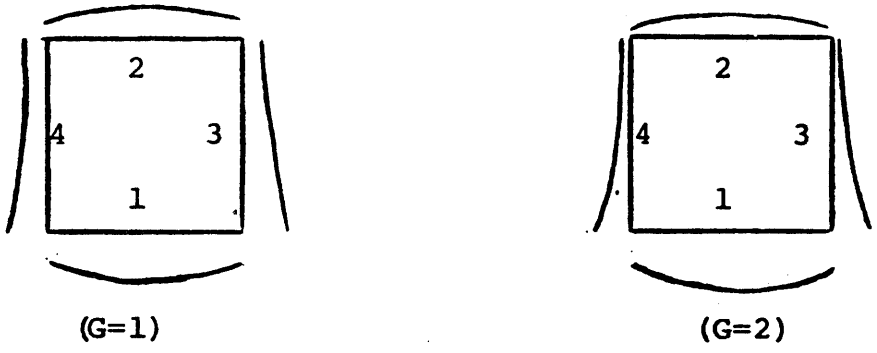

Incoming Group Two Partial Current (G'=2)

Outgoing Group Partial Current Shapes Resulting from Flat Unit Incoming Group Partial Currents Along Face 1.

FIGURE 3.1

Representation of Cell Calculation for Two Energy Groups and a Quarter-Symmetric Assembly

$J_g^{\ell'}(in,i)$'s is not required. To show that this is true, Eq. (2.6) can be rewritten as

$$\bar{\Sigma}_{\alpha g}^{(i)} = \frac{J_2^1(in,i) \sum_{\ell'=1}^{4} \sum_{g'=1}^{G} I_{gg'}^{\ell'}(\alpha,i) f_{g'}^{\ell'}(i)}{J_2^1(in,i) \sum_{\ell'=1}^{4} \sum_{g'=1}^{G} \bar{\phi}_{gg'}(i) f_{g'}^{\ell'}(i)}$$

$$= \frac{\sum_{\ell'=1}^{4} \sum_{g'=1}^{G} I_{gg'}^{\ell'}(\alpha,i) f_{g'}^{\ell'}(i)}{\sum_{\ell'=1}^{4} \sum_{g'=1}^{G} \bar{\phi}^{\ell'}_{gg'}(i) f_{g'}^{\ell'}(i)} \qquad (3.1)$$

=

where $f_g^{\ell'}(i) = J_g^{\ell'}(in,i)/J_2^1(in,i)$. Note that $f_2^1(i)=1$. Also, $J_2^1(in,i)$ is chosen arbitrarily. Any one of the $J_g^{\ell'}(in,i)$'s could have been factored out of Eq. (2.6) and Eq. (3.1) would still be valid with the $f_g^{\ell'}(i)$'s redefined accordingly. Thus, for the purpose of calculating $\bar{\Sigma}_{\alpha g}^{(i)}$ by Eq. (3.1), the $J_g^{\ell'}(in,i)$'s (actually all but one) must be known only as a multiplicative factor of one of the incoming group partial currents. This fact will be useful in the following scheme.

Let the incoming partial current vector along face ℓ'

of assembly i be denoted by $[J^{\ell'}_{in}]_i$ where

$$[J^{\ell'}_{in}]_i = \text{Col}\ \{J^{\ell'}_1(in,i), J^{\ell'}_2(in,i), \ldots, J^{\ell'}_G(in,i)\}. \quad (3.2)$$

The incoming group partial currents for each face are represented as vectors in Figure 3.2.

The outgoing partial current vector for face 1, $[J^{\ell}_{out}]_i$, can be written in terms of the four incoming partial current vectors using the response matrices of the assembly:

$$[J^{\ell}_{out}]_i = [R^{\ell 1}]_i [J^1_{in}]_i + [R^{\ell 2}]_i [J^2_{in}]_i + [R^{\ell 3}]_i [J^3_{in}]_i +$$

$$[R^{\ell 4}]_i [J^4_{in}]_i \quad ; \quad (\ell = 1,2,3,4) \quad (3.3)$$

where $[R^{\ell\ell'}]_i = \{R^{\ell\ell'}_{gg'}(i)\}$, a G x G matrix ($\ell = 1,2,3,4$; $\ell' = 1,2,3,4$).

The $R^{\ell\ell'}_{gg'}(i)$ element is defined in Eq. (2.1). Each $R^{\ell\ell'}_{gg'}(i) \geq 0$.

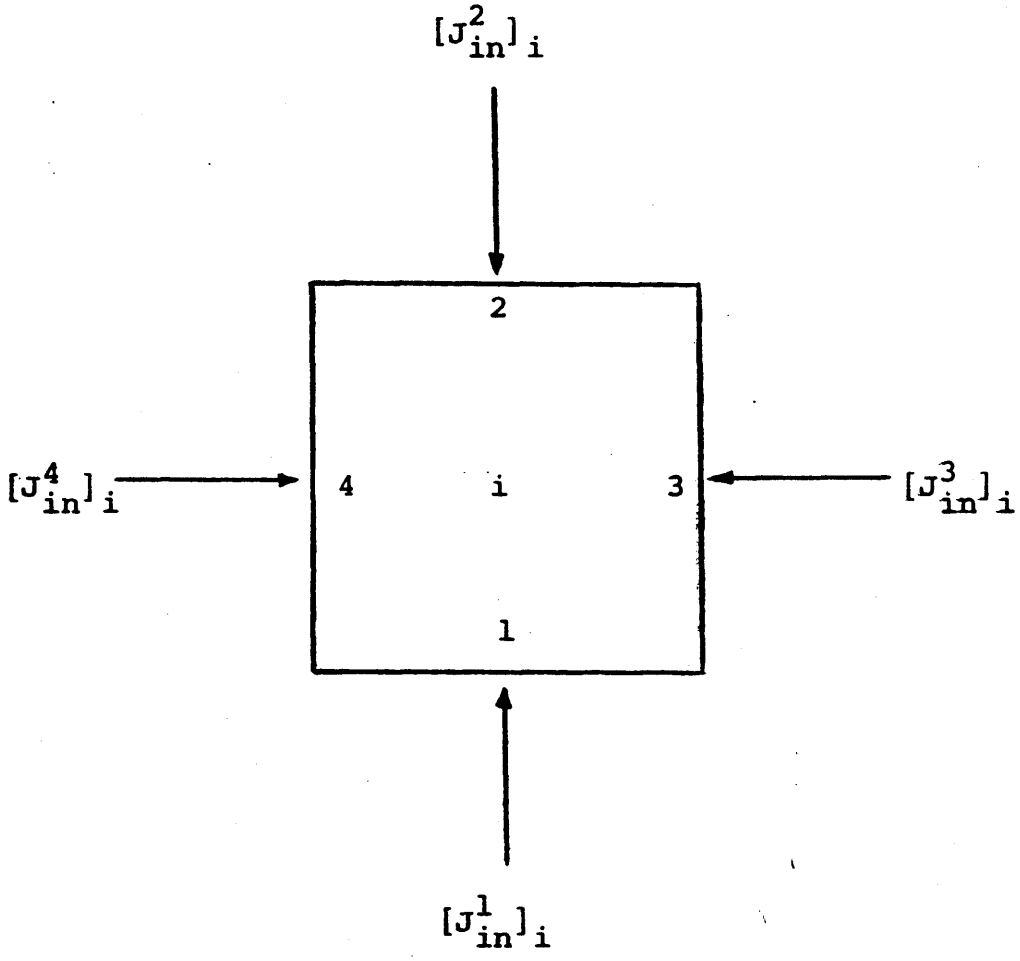

FIGURE 3.2

Representation of Group Partial Currents

Entering an Assembly

A supermatrix $[R]_i$ is now defined such that

$$[R]_i = [R^{\ell\ell'}]_i \quad (\ell=1,2,3,4;\ \ell'=1,2,3,4). \tag{3.4}$$

The matrix $[R]_i$ is a 4G x 4G matrix. The relation between the incoming and outgoing partial current vectors can be written as

$$[J_{out}]_i = [R]_i[J_{in}]_i \ . \tag{3.5}$$

where

$$[J_{out}]_i = \text{Col}\{[J^1_{out}]_i, [J^2_{out}]_i, [J^3_{out}]_i, [J^4_{out}]_i\}$$

and

$$[J_{in}]_i = \text{Col}\{[J^1_{in}]_i, [J^2_{in}]_i, [J^3_{in}]_i, [J^4_{in}]_i\}.$$

$[J_{out}]_i$ and $[J_{in}]_i$ are 4G column vectors.

Each incoming partial current vector for face 1', $[J^{\ell'}_{in}]_i$, can be written in terms of the outgoing partial current vector for face 1', $[J^{\ell'}_{out}]_i$, in terms of an albedo matrix:

$$[J^{\ell'}_{in}]_i = [\alpha^{\ell'}]_i [J^{\ell'}_{out}]_i \tag{3.6}$$

where

$$[J^{\ell'}_{out}]_i = \text{Col}\ [J^{\ell'}_1(\text{out},i), J^{\ell'}_2(\text{out},i), \ldots,$$

$$J^{\ell'}_G(\text{out},i)]$$

and

$$[\alpha^{\ell'}]_i \equiv \{\alpha^{\ell\ell'}_{gg'}(i)\}\ ,\ \text{a G x G matrix.}$$

The elements $\alpha^{\ell'}_{gg'}(i)$ are such that

$\alpha^{\ell'}_{gg'}(i)$= the fraction of the integrated group g' (g'=1,2,...,G) partial current leaving face 1' of assembly i which appears in energy group g (g=1,2,...,G) and enters face 1'.

Note that $\alpha^{\ell'}_{gg'}(i)$ will be a real number greater than or equal to zero.

The incoming partial current vector for assembly i, $[J_{in}]_i$, can be related to $[J_{out}]_i$ by a diagonal supermatrix $[A]_i$

as follows:

$$[J_{in}]_i=[A]_i[J_{out}]_i \tag{3.8}$$

where

$$[A]_i \equiv \begin{bmatrix} [\alpha^1]_i & & & \\ & [\alpha^2]_i & 0 & \\ & 0 & [\alpha^3]_i & \\ & & & [\alpha^4]_i \end{bmatrix} \tag{3.9}$$

Eqs. (3.5) and (3.8) are combined such that

$$[J_{in}]_i=[W]_i[J_{in}]_i \tag{3.10}$$

where

$$[W]_i \equiv [A]_i[R]_i \quad . \tag{3.11}$$

Eq. (3.10) will have a non-zero solution only for a certain value of the 4G x 4G matrix $[W]_i$. It is highly unlikely that the (4G x 4G) elements of $[W]_i$ will be such that

Eq. (3.10) will have a non-trivial solution. However, Eq. (3.10) can be treated as an eigenvalue problem such that

$$\gamma[J_{in}]_i=[W]_i[J_{in}]_i \tag{3.12}$$

where, if the reactor is critical and the albedoes are correct, the eigenvalue γ will equal unity. The elements of $[W]_i$ ($\equiv[A]_i[R]_i$) ≥ 0 because all $\alpha^{\ell'}_{gg'}(i)$ and $R^{\ell\ell'}_{gg'}(i) \geq 0$. Since $[W]_i$ is nonnegative, it has a nonnegative real eigenvalue γ, and the corresponding eigenvector, $[J_{in}]_i$, has nonnegative components, not all zero[13]. The incoming group partial current vector entering assembly i, $[J_{in}]_i$, can be determined within a multiplicative constant by solving this eigenvalue problem. This is enough information for the purpose of calculating $\bar{\Sigma}^{(i)}_g$'s as previously discussed (see Eq. (3.1)).

The calculation of $[J_{in}]_i$ using Eq. (3.12) requires the knowledge of $[\alpha^{\ell'}]_i$ for $\ell'=1,2,3,4$. A knowledge of the exact values of the $[\alpha^{\ell'}]_i$ elements would require a full-core solution to the group diffusion equations. Also, the values of the $[\alpha^{\ell'}]_i$'s ($\ell=1,2,3,4$) may be different for each assembly, and they depend upon the position of assembly i within the reactor. To estimate the elements of $[\alpha^{\ell'}]_i$

without solving the full-core problem, we make the following assumption. Consider Figure 3.3 which shows an assembly i surrounded by four adjacent assemblies numbered one through four. $[\alpha^1]_i$ is the albedo matrix relating the outgoing partial current vector on face 1 of Assembly i to the incoming partial current vector on face 1 of Assembly i by the relationship given in Eq. (3.6). The matrix $[\alpha^1]_i$ is dependent upon the composition of Assembly 1 as well as the actual boundary conditions along the three faces of Assembly 1 which are not adjacent to Assembly i. Since these boundary conditions cannot be determined exactly without solving the full-core problem, we assume that, for Assembly 1, the net group current is approximately zero across each face not adjacent to Assembly i. Thus,

$$[J^{\ell}_{out}]_1 = [J^{\ell}_{in}]_1 \qquad \text{for } \ell = \text{faces not adjacent to i.} \tag{3.13}$$

Once this assumption is made, the elements of $[\alpha^1]_i$ can be calculated from the knowledge of the response matrices of Assembly 1 as we shall show.

Let Assembly 1 in Figure 3.3 be isolated from Assembly i and let the faces of Assembly 1 be numbered as shown in Figure 3.3. Note that face 1 of Assembly 1, as depicted in Figure 3.3, is adjacent to face 1 of Assembly i. Thus,

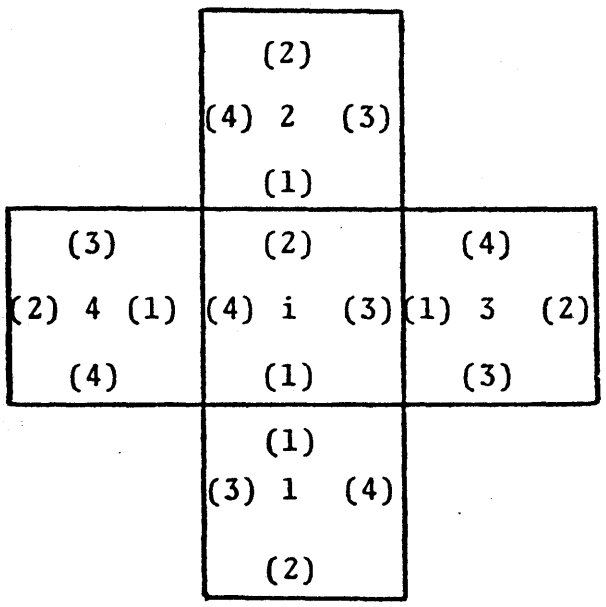

FIGURE 3.3

Representation of Assembly and Its Four Adjacent Neighbors

$$[J^1_{in}]_{\text{Assembly } 1} = [J^1_{out}]_{\text{Assembly } i} \tag{3.14a}$$

$$[J^1_{out}]_{\text{Assembly } 1} = [J^1_{out}]_{\text{Assembly } i} \cdot \tag{3.14b}$$

The matrix $[\alpha^1]_i$ is sought such that $[J^1_{in}]_i = [\alpha^1]_i [J^1_{out}]_i$, or using Eq. (3.14a)

$$[J^1_{in}]_i = [\alpha^1]_i [J^1_{in}]_i \cdot \tag{3.15}$$

$[J^1_{out}]_1$ is first written as

$$[J^1_{out}]_1 = [R^{11}]_1 [J^1_{in}]_1 + [R^{12}]_1 [J^2_{in}]_1 +$$

$$[R^{13}]_1 [J^3_{in}]_1 + [R^{14}]_1 [J^4_{in}]_1 \cdot \tag{3.16}$$

The use of Eq. (3.13) then gives

$$[J^1_{out}]_1 = [R^{11}]_1 [J^1_{in}]_1 + [D]_1 [C]_1 \tag{3.17}$$

where

$$[C]_1 \equiv \text{Col}\{ [J^2_{out}]_1, [J^3_{out}]_1, [J^4_{out}]_1 \} \tag{3.18}$$

and

$$[D]_1 \equiv \{[R^{12}]_1[R^{13}]_1[R^{14}]_1\} \ . \tag{3.19}$$

Equations similar to Eq. (3.17) can be written for each $[J^m_{out}]_1$ (m=2,3,4) in terms of $[J^1_{in}]$, the $[J^m_{out}]_1$ (for m=2,3,4), and the response matrices of Assembly 1. The resulting group of equations can then be written as

$$[C]_1=[L]_1[J^1_{in}]_1+[P]_1[C]_1 \tag{3.20}$$

where $[C]_1$ is defined by Eq. (3.18),

$$[L]_1 \equiv \text{Col}\{[R^{21}]_1,[R^{31}]_1,[R^{41}]_1\} \tag{3.21}$$

and

$$[P]_1 \equiv \begin{bmatrix} [R^{22}]_1 & [R^{23}]_1 & [R^{24}]_1 \\ [R^{32}]_1 & [R^{33}]_1 & [R^{34}]_1 \\ [R^{42}]_1 & [R^{43}]_1 & [R^{44}]_1 \end{bmatrix} \tag{3.22}$$

The matrix $[C]_1$ can be determined from Eq. (3.2) to be

$$[C]_1 = \left[[I]-[P]_1\right]^{-1}[L]_1[J^1_{in}]_1 \quad . \tag{3.23}$$

Combining Eqs. (3.23) and (3.17) yields

$$[J^1_{out}]_1 = \left[[R^{11}]_1+[D]_1[[I]-[P]_1]^{-1}[L]_1\right][J^1_{in}]_i . \tag{3.24}$$

But $[J^1_{out}]_1=[J^1_{in}]_i$ from Eq. (3.14b). Therefore,

$$[J^1_{in}]_i = \left[[R^{11}]_1+[D]_1[[I]-[P]_1]^{-1}[L]_1\right][J^1_{in}]_1 \quad . \tag{3.25}$$

It is apparent from comparing Eq. (3.25) to Eq. (3.15) that

$$[\alpha^1]_i = \left[[R^{11}]_1+[D]_1[[I]-[P]_1]^{-1}[L]_1\right] \quad . \tag{3.26}$$

The albedo matrix for each of the other faces of Assembly i shown in Figure 3.3, $[\alpha^\ell]_i$ (ℓ=2,3,4), are found in the same manner as $[\alpha^1]_i$. Once the $[\alpha^\ell]_i$'s are determined they are used in Eq. (3.11).

The evaluation of $[\alpha^1]_i$, a G x G matrix, requires that

the inverse of $\left[[I]-[P]_1\right]$, a 3G x 3G matrix, be calculated. For two energy groups the calculation of $[\alpha^1]_i$ takes very little computer time.

For assembly faces adjacent to a water reflector, shroud and reflector, etc., alternative means for obtaining the corresponding $[\alpha^1]_i$ are available. For example, expressions for two-group albedoes for various water reflector and shroud plus reflector geometries have been determined by Kalambokas[14]. These albedoes obey Eq. (3.6) and are used in Eq. (3.11) as are the $[\alpha^\ell]_i$'s calculated from Eq. (3.26).

The homogenization procedure for calculating equivalent group diffusion constants as a function of assembly position within the reactor is sufficiently complex that a review of the technique may be helpful at this point.

The homogenization scheme can be broken into four distinct stages:

1) Calculate the current response matrices and the integrated reaction rate response matrices for each different assembly composition. For assemblies with quarter-assembly symmetry only the response matrices for neutrons incident upon one face are required. The response matrices are calculated in the cell calculation and are inexpensive to determine. A typical reactor is

made up of only three or four different assembly compositions and therefore only the corresponding number of cell calculations are performed.

2) Calculate the albedo matrices, $[\alpha^{\ell}]^{k}$ (l=1,2,3,4), for each different assembly composition k using Eq. (3.26). Note that, because of the approximations used to determine the $[\alpha^{\ell}]^{k}$'s (Eq. (3.13)) and because $[\alpha^{\ell}]$ is therefore dependent only upon the assembly composition, the $[\alpha^{\ell}]^{k}$'s need be determined only for each different assembly composition and not for each location i. Also, $[\alpha^{\ell}]^{k}$ will be identical for each l (l=1,2,3,4) for assemblies with quarter-assembly symmetry. Thus, only one $[\alpha^{\ell}]^{k}$ need be calculated for each composition k displaying such symmetry. For example, for a reactor having three different assembly compositions in which all assemblies are quarter-symmetric, only three distinct $[\alpha^{\ell}]^{k}$ matrices are calculated using Eq. (3.26). Other $[\alpha^{\ell}]^{k}$'s may be needed for the assembly-reflector interfaces. The corresponding albedo matrices are determined by alternate means[14] as previously pointed out.

3) The $[J^{\ell}_{in}]_{i}$'s are calculated from Eq. (3.12) once the $[\alpha^{\ell}]^{k}$'s are obtained from step 2. The $[\alpha^{\ell}]_{i}$'s

of assembly i are the $[\alpha^{\ell}]^{k}$'s of the corresponding adjacent material k. For example, as depicted in Figure 3.3, $[\alpha^{1}]_{i}$ of Assembly i is the $[\alpha^{1}]^{k}$ of Assembly 1 where $[\alpha^{1}]^{k}$ of Assembly 1 has been calculated in step 2. Likewise, if side 1 of Assembly i is adjacent to water rather than another assembly, $[\alpha^{1}]_{i}=[\alpha^{1}]^{k=water}$ where $[\alpha^{1}]^{k=water}$ is the albedo matrix of the water reflector as calculated using Kalambokas's results. Note that step 3 is the first stage in the calculation of the $\bar{\Sigma}_{\alpha g}^{(i)}$'s where assembly position is considered. A set of $[J_{in}^{\ell}]_{i}$'s will be determined uniquely for each assembly position i. (Note, however, that for repeating assembly placements in a large reactor, such as a checkerboard array, a particular assembly composition might be surrounded identically for several different positions i. In such cases the $[J_{in}^{\ell}]_{i}$'s will be identical for several values of i and $[J_{in}^{\ell}]_{i}$ for $\ell=1,2,3,4$ must be determined only once for all those positions.)

4) The homogenized group cross sections, $\bar{\Sigma}_{\alpha g}^{(i)}$, are calculated using Eq. (2.6) since all $[J_{in}^{\ell}]_{i}$'s are known from the previous step. The determination of the $\bar{\Sigma}_{\alpha g}^{(i)}$'s still requires the knowledge of the

$\bar{\phi}^{(i)}_{gg'}$'s. The $\bar{\Sigma}^{(i)}_{\alpha g}$'s and $\bar{D}^{(i)}_{g}$'s can be calculated by the double-iterative search scheme outlined in Chapter 2. However, a scheme for determining $\int_{V_i} \bar{\phi}_g(\underline{r})dV$ will be described in Section 3.3, thereby eliminating the double-iterative search.

One significant point concerning the calculation of the $\bar{\Sigma}^{(i)}_{\alpha g}$'s using Eq. (2.6) should be mentioned. For symmetric assemblies the evaluation of the $\bar{\Sigma}^{(i)}_{\alpha g}$'s may be written such that

$$\bar{\Sigma}^{(i)}_{\alpha g} = \frac{\sum_{\ell'=1}^{4} \sum_{g'=1}^{G} I_{gg',(\alpha,i)} J^{\ell'}_{g',(in,i)}}{\sum_{\ell'=1}^{4} \sum_{g'=1}^{G} \bar{\phi}_{gg',(i)} J^{\ell'}_{g',(in,i)}} \tag{3.27a}$$

where $I_{gg',(\alpha,i)}$ and $\bar{\phi}_{gg',(i)}$ are without superscripts. If the $J^{\ell'}_{g',(in,i)}$ are identical for all ℓ' then the above expressions reduces to

$$\bar{\Sigma}^{(i)}_{\alpha g} = \frac{\sum_{g'=1}^{G} I_{gg',(\alpha,i)} J_{g',(in,i)}}{\sum_{g'=1}^{G} \bar{\phi}_{gg',J_{g'},(in,i)}} \tag{3.27b}$$

where there is not a superscript on $J_{g'}(in,i)$. Or if

$$\sum_{\ell'=1}^{2} [J_{in}^{\ell'}]_i = \sum_{\ell'=3}^{4} [J_{in}^{\ell'}]_i \quad \text{(see Fig. 3.2) then Eq. (3.27a)}$$

reduces to

$$\bar{\Sigma}_{\alpha g}^{(i)} = \frac{\sum_{\ell'=1}^{2} \sum_{g'=1}^{2} I_{gg'}(\alpha,i) J_{g'}^{\ell'}(in,i)}{\sum_{\ell'=1}^{2} \bar{\phi}_{gg'}(\alpha,i) J_{g'}^{\ell'}(in,i)} \quad . \tag{3.27c}$$

These expressions reduce the amount of computation required to calculate the $\bar{\Sigma}_{\alpha g}^{(i)}$'s, and will prove useful for most practical reactor problems. Most important, however, is that the above three relations will be needed for the evaluation of $\int_{V_i} \bar{\phi}_g(\underline{r})\,dV$ as described in Section 3.3.

The albedo matrices provide a means for calculating the incoming group partial currents for an assembly (within a multiplicative factor) through the use of Eqs. (3.11) and (3.12). One interesting observation is noteworthy. The previous technique assumes $[J_{in}^{\ell}]_i$ identical for all ℓ and calculates a value of the incoming group 1 to group 2 partial current ratio, using Eq. (2.9). It can be shown (see Appendix A) that equating each $[\alpha^{\ell}]_i$ of assembly i

to the G x G identity matrix and solving Eqs.(3.11) and (3.12) in terms of the response matrices results in an expression for X identical to Eq. (2.9). Thus, the semi-infinite medium method outlined in Chapter 2 for obtaining the two-group $[J_{in}]_i$ can be viewed as a special case of the present method. But, the use of the albedo matrices calculated from Eq. (3.26) for assembly-assembly interfaces or those found using Kalambokas's method for assembly-reflector interfaces will result in a better representation of the true boundary conditions of the assembly.

The albedo matrices of the two BWR assembly compositions shown in Fig. 2.1 were computed and are listed in Table 3.1. These are the $[\alpha^{\ell}]^k$ matrices of each different assembly composition. The $[\alpha^{\ell}]_i$'s used in Eq. (3.11) are the $[\alpha^{\ell}]^k$'s of the material surrounding assembly i. Note that the matrices listed in Table 3.1 are much different from the identity matrix, and only the $[\alpha^1]^k$ elements are listed since the other $[\alpha^{\ell}]^k$'s (ℓ=2,3,4) will be identical to $[\alpha^1]^k$ because of assembly symmetry.

Four different PWR assembly compositions are shown in Fig. 3.4. Note that these assemblies are larger than the BWR assemblies. Assembly types F and E have shim rods in addition to the five control rod channels. The control rod channel is filled with water in all assembly types except assembly D_o^w. The corresponding $[\alpha^{\ell}]^k$'s for each assembly

TABLE 3.1

Material Albedoes - BWR Compositions*

	Assembly A	Assembly B
α^1_{11}	8.7582-1	1.0092+0
α^1_{12}	7.4347-1	9.5021-1
α^1_{21}	7.7504-2	1.1372-1
α^1_{22}	3.9796-1	4.4841-1

*The assemblies are quarter-symmetric and the albedo matrices $[\alpha^\ell]_i$ are identical for ℓ=1,2,3,4. Therefore only the elements of $[\alpha^1]_i$ are listed. The notation $\alpha^\ell_{gg'}$ refers to Eq. (3.7). Assemblies A and B refer to those shown in Figure 2.1.

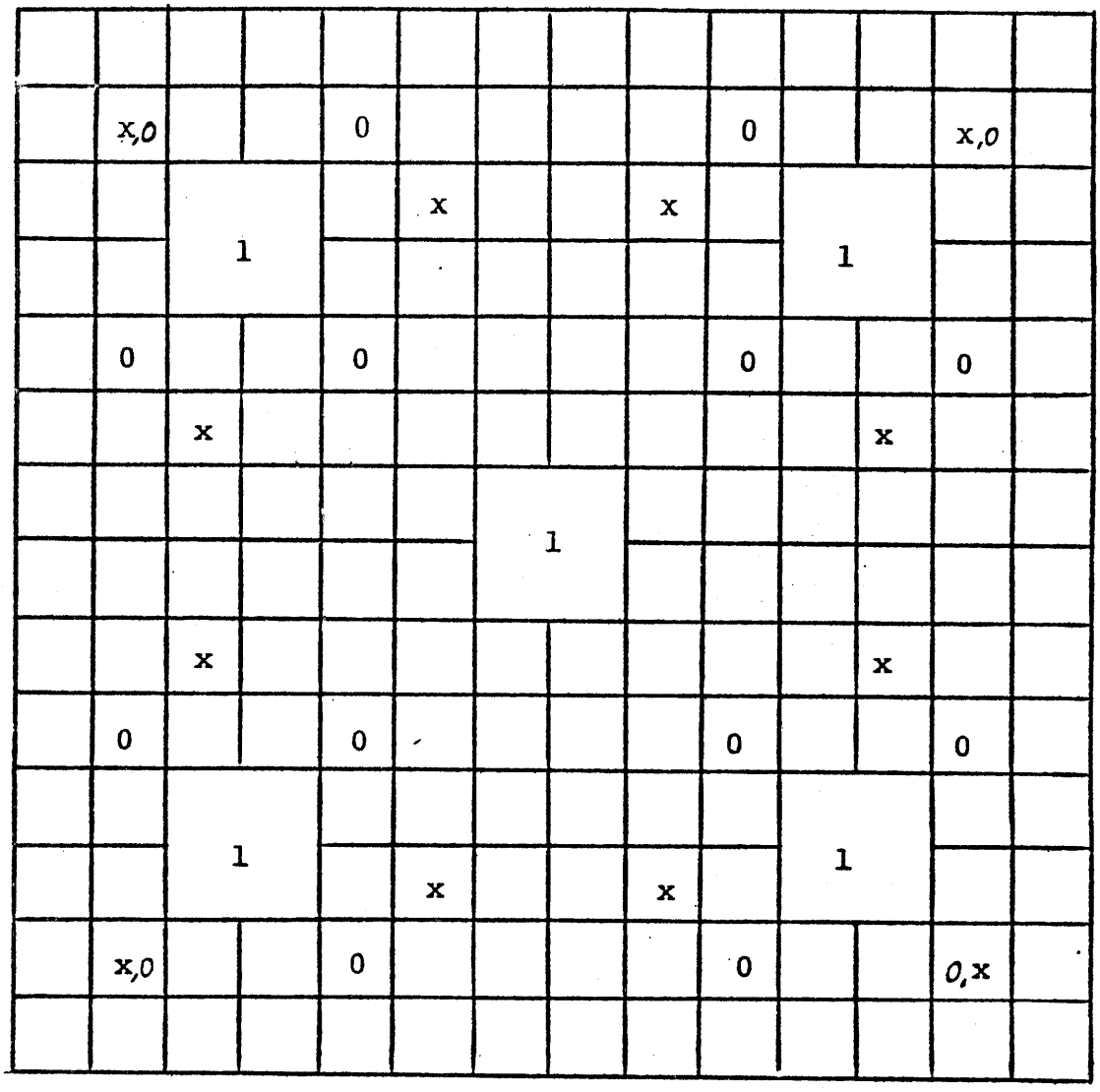

Assembly is 20.6248 cm x 20.6248 cm with 196 square cells each 1.4732 cm x 1.4732 cm.

Assembly Type	Material 1	Shim Notation
F_{12}	water	x
E_{16}	water	0
D_o	water	no shims
D_o^w	control rod	no shims

Remaining material is fuel. Nuclear properties of the fuel, shims, water and control rod for assemblies are listed in Appendix C.

FIGURE 3.4 - Typical PWR Compositions

type were calculated and are listed in Table 3.2. The assemblies are quarter-symmetric and only the $[\alpha^{l}]^{k}$'s need by calculated.

The technique described in this section for calculating EGDC provides a means for determining the $[J^{\ell'}_{in}]_i$'s as a function of reactor position i. In addition, the actual technique is independent of assembly position. Only the $[J^{\ell}_{in}]_i$'s used to compute the cross sections change from position to position, and these depend upon the albedo matrices of the surrounding material. The albedo matrices in turn depend only upon assembly composition. The last stage of the homogenization proceudre calculates $\bar{\Sigma}^{(i)}_{\alpha g}$ by solving Eq. (2.6). This solution requires a knowledge of the $\bar{\phi}^{\ell'}_{gg},(i)$'s. In the following section a method is presented that eliminates the iterative search for $\int_{V_i} \bar{\phi}_g(\underline{r})\,dV$.

3.3 A Method for Predetermining the Integral of the Flux-Shape Resulting from the Use of EGDC

The previous scheme for calculating EGDC use a double-iterative search. The group diffusion coefficients were chosen and the $\bar{\Sigma}^{(i)}_{\alpha g}$'s were found by an iterative determination of $\int_{V_i} \bar{\phi}(\underline{r})\,dV$. New diffusion coefficients were found by matching the largest response matrix elements and the

TABLE 3.2

Material Albedoes - PWR Compositions*

	Assembly F_{12}	Assembly E_{16}	Assembly D_0	Assembly D_0^W
α_{11}^1	1.1132+0	1.2438+0	1.2273+0	5.8779-1
α_{12}^1	9.6944-1	1.0888+0	1.0027+0	4.9052-1
α_{21}^1	1.2589-1	1.7219-1	1.8348-1	8.0729-2
α_{22}^1	4.5659-1	5.2922-1	5.5508-1	4.6445-1

*The assemblies are quarter-symmetric and the albedo matries $[\alpha^{\ell}]_i$ are identical for ℓ=1,2,3,4. Therefore only the elements of $[\alpha^1]_i$ are listed. The notation α_{gg}^{ℓ}, refers to Eq. (3.7). Assemblies F_{12},E_{16},D_0 and D_0^W refer to those shown in Figure 3.4.

$\bar{\Sigma}_{\alpha g}^{(i)}$'s were recomputed for these new set of $\bar{D}_g$'s. Then new $\bar{D}_g$'s were found for the recomputed $\bar{\Sigma}_{\alpha g}^{(i)}$'s. The double-iterative search was found to converge to a set of $\bar{\Sigma}_{\alpha g}^{(i)}$'s and $\bar{D}_g^{(i)}$'s that reproduce the largest response matrix elements and the $\int_{V_i} \bar{\phi}_g(\underline{r})dV$ used in calculating the $\bar{\Sigma}_{\alpha g}^{(i)}$'s.

In this section a method is presented which eliminates the step of computing $\int_{V_i} \bar{\phi}_g(\underline{r})dV$ iteratively.

The flux shape in assembly i resulting from the use of EGDC in the full-core problem will closely match the flux shape in assembly i resulting from the cell calculation provided that the boundary conditions used in the cell calculation closely match the boundary conditions of the homogeneous full-core solution. Recall that we also require that incoming group partial currents of the homogeneous assembly match those of the heterogeneous assembly. Therefore the incoming group partial currents of the homogeneous cell calculation will be the same as those of the heterogeneous cell calculation. This means that the $[J_{in}^{\ell}]_i$'s calculated for the heterogeneous assembly by the methodology outlined in Section 3.2 will be used as the boundary condition for the homogeneous assembly. This fact is mentioned since a homogeneous assembly calculation must be carried out in

order to calculate $\int_{V_i} \bar{\phi}_g(\underline{r})dV$ iteratively. And for the purpose of computing $\int_{V_i} \bar{\phi}_g(\underline{r})dV$ in a non-iterative manner the heterogeneous assembly boundary conditions will be matched.

It should be pointed out that the "true" integrated reaction rates of the heterogeneous assembly are calculated using Eq. (2.4) and this is the same expression used in the numerator of the ratio in Eq. (2.6). Thus, after the response matrices of the heterogeneous assembly are calculated and the $[J^{\ell}_{in}]_i$'s are determined from Eq. (3.12), a heterogeneous assembly calculation using the $[J^{\ell}_{in}]_i$'s as the fixed surface source is <u>not</u> performed since enough information is available for calculating the heterogeneous reaction rates from Eq. (2.4). Likewise, once the $[J^{\ell}_{in}]_i$'s are determined, the $[J^{\ell}_{out}]_i$'s of the heterogeneous assembly are calculated using Eq. (2.3).

The flux shape in the homogeneous assembly will be relatively smooth. This fact suggests that $\bar{\phi}_g(\underline{r})$ within the homogeneous assembly can be expanded as a polynomial function. Since the $J^{\ell}_g(in,i)$'s and $J^{\ell}_g(out,i)$'s yield values of the average group fluxes and their normal derivatives for the assembly surfaces, $\bar{\phi}_g(\underline{r})$ can be estimated by fitting to products of Cubic Hermite polynomials.

Consider the assembly shown in Figure 3.5. Let the integrated group flux along face ℓ, $\overset{\gamma\ell}{\phi}_g$, and the integrated group net current in the outward normal direction, $\overset{\gamma\ell}{J}_g$, be defined as follows:

$$\overset{\gamma 1}{\phi}_g \equiv \int_0^{h_x} \phi_g(x,0)\,dx \tag{3.28a}$$

$$\overset{\gamma 2}{\phi}_g \equiv \int_0^{h_x} \phi_g(x,h_y)\,dx \tag{3.28b}$$

$$\overset{\gamma 3}{\phi}_g \equiv \int_0^{h_y} \phi_g(h_x,y)\,dy \tag{3.28c}$$

$$\overset{\gamma 4}{\phi}_g \equiv \int_0^{h_y} \phi_g(o,y)\,dy \tag{3.28d}$$

$$\overset{\gamma 1}{J}_g \equiv -\int_0^{h_x} J_{gy}(x,0)\,dx \tag{3.29a}$$

$$\overset{\gamma 2}{J}_g \equiv \int_0^{h_x} J_{gy}(x,h_y)\,dx \tag{3.29b}$$

$$\overset{\gamma 3}{J}_g \equiv \int_0^{h_y} J_{gx}(h_x,y)\,dy \tag{3.29c}$$

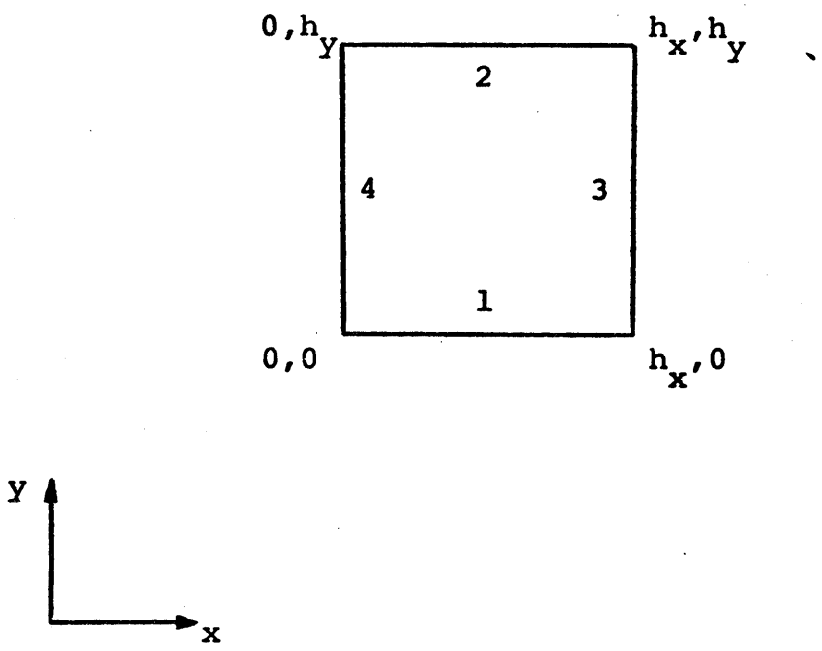

FIGURE 3.5
Representation of Assembly Notation
Used in Cubic-Hermite Expressions

$$\tilde{J}_g \equiv -\int_0^{h_y} J_g y(0,y)\,dy \qquad (3.29d)$$

where the $\phi_g(x,0)$, $J_g y(x,0)$, etc. are group fluxes and net currents along the surfaces of the heterogeneous assembly (calculated from the known values of the $J_g^{\ell}(in,i)$ and $J_g^{\ell}(out,i)$'s). The negative sign in Eqs. (3.29a) and (3.29d) is required since $\tilde{J}_g^{\ell}$ is the integral of the group g net current leaving face ℓ in the outward normal direction and $J_g y(x,0)$ and $J_g x(y,0)$ are the group g net currents along faces 1 and 4 respectively in the positive x and y directions which are the inward normal direction for faces 1 and 4.

The integral of the group flux and group current along the surface of the homogeneous node are required to match those of the heterogeneous node. Therefore, for the homogeneous assembly, we expand the integral of the group flux in the y-direction in the x-direction in terms of the integrated group fluxes and currents along faces 3 and 4 such that

$$\int_0^{h_y} \bar{\phi}_g(x,y)\,dy = \tilde{\phi}_g^4 u_0^{0+}(x) + \tilde{\phi}_g^3 u_{h_x}^{0-}(x) + \frac{\tilde{J}_g^4}{D_g} u_0^{1+}(x) - \frac{\tilde{J}_g^3}{D_g} u_{h_x}^{1-}(x) \qquad (3.30)$$

where the $u_0^{0+}(x)$ etc. are the Cubic Hermite basis functions (see Appendix B). In a similar manner, the integral of the flux in the x-direction is expanded in the y-direction such that

$$\int_0^{h_x} \bar{\phi}_g(x,y)\,dx = \tilde{\phi}_g^1 w_0^{0+}(y) + \tilde{\phi}_g^2 w_{h_y}^{0-}(y) + \frac{\tilde{J}_g^1}{D_g} w_0^{1+}(y) - \frac{\tilde{J}_g^2}{D_g} w_{h_y}^{1-}(y) \qquad (3.31)$$

where the $w_0^{1+}(y)$ etc. are also defined in Appendix B.

Integrating Eq. (3.30) from 0 to h_x and Eq. (3.31) from 0 to h_y gives the following two relations:

$$\int_0^{h_x}\int_0^{h_y} \bar{\phi}_g(x,y)\,dxdy = \frac{h_x}{2}[\tilde{\phi}_g^4 + \tilde{\phi}_g^3] + \frac{h_x^2}{12D_g}[\tilde{J}_g^4 + \tilde{J}_g^3] \qquad (3.32)$$

and

$$\int_0^{h_x}\int_0^{h_y} \bar{\phi}_g(x,y)\,dxdy = \frac{h_y}{2}[\tilde{\phi}_g^1 + \tilde{\phi}_g^2] + \frac{h_y^2}{12D_g}[\tilde{J}_g^1 + \tilde{J}_g^2] \quad . \qquad (3.33)$$

These expressions for $\int_0^{h_x}\int_0^{h_y}\bar{\phi}_g(x,y)dxdy$ are the $\int_{V_i}\bar{\phi}_g(\underline{r})dV$ that we seek for use in Eq. (1.3). For the purpose of calculating EGDC by the response matrix scheme, the $\overset{\gamma\ell}{\phi}_g$'s and $\overset{\gamma\ell}{J}_g$'s are calculated in terms of the response matrices of the heterogeneous assembly. However, there are now two expressions for $\int_{V_i}\bar{\phi}_g(\underline{r})dV$. The integral of the flux as computed from Eq. (3.32) uses information of the flux and current along the two faces of the assembly, and the integral as computed from Eq. (3.33) uses information pertaining to the other two faces. The optimum procedure for determining $\int_{V_i}\bar{\phi}_g(\underline{r})dV$ would be one which uses the available information about the flux and current along all four faces of the assembly.

In addition, it should be pointed out that the use of Eq. (3.32) and Eq. (3.33) requires the value of D_g. The proper value of D_g to use in these equations is not clear. The values of the $\bar{D}_g^{(i)}$'s found by matching the largest response matrix elements cannot be determined until the homogenized cross sections are known. In fact, matching the "true" $\int_{V_i}\bar{\phi}_g(\underline{r})dV$ (found by the double-iterative search) by choosing various values of D_g results in a value of D_g that is not even close in value to the "true" $\bar{D}_g$. If $\int_{V_i}\bar{\phi}_g(\underline{r})dV$

as determined by Eq. (3.32) or (3.33) is only slightly dependent upon the D_g, then any reasonable value of D_g could be used, but this dependence was found to be significant. Because of the lack of a value for D_g and because each of the above equations use only half of the available surface information, the use of only one of the above equations to calculate $\int_{V_i} \bar{\phi}_g(\underline{r})dV$ is theoretically unsound. Indeed,

the use of either Eq. (3.32) or Eq. (3.33) alone to compute $\int_{V_i} \bar{\phi}_g(\underline{r})dV$ was shown to give inaccurate results.

A successful approach was found to be one which uses both equations. The integral of the group flux as computed from Eq. (3.32) or (3.33) is a linear function of $1/D_g$. Note however that for a quarter-symmetric assembly i, if

$\sum_{\ell'=1}^{2} [J_{in}^{\ell'}]_i = \sum_{\ell'=3}^{4} [J_{in}^{\ell'}]_i$ (see Fig. 3.2) or if the $[J_{in}^{\ell'}]_i$ is

the same for all 1' 's, the two expressions (3.32) and (3.33) will be identical. But for either of these two situations, two independent expressions can be determined since the $\bar{\Sigma}_{\alpha g}^{(i)}$'s can be computed using Eq. (3.27b) or (3.27c). Use of either Eq. (3.27b) or (3.27c) will guarantee that Eqs. (3.32) and (3.33) will be distinct. In addition, it is highly unlikely that, for non-symmetric assemblies, Eqs. (3.32) and (3.33) will not be distinct. Thus, the scheme to be described first

requires that, if so needed, the $\bar{\Sigma}_{\alpha g}^{(i)}$'s be computed using Eq. (3.27b) or (3.27c).

The two linear functions of Eqs. (3.32) and (3.33) are plotted in Fig. 3.6 for a rodded BWR assembly (Fig. 2.1) of an infinite repeating lattice. (Note that in this case, for example, all $[J_{in}^{\ell'}]$'s are the same for $\ell'=1,2,3,4$ and Eq. (3.27b) is used to insure two distinct linear functions for $\int_{V_i} \bar{\phi}_g(\underline{r})dV$.) The two straight lines representing $\int_{V_i} \bar{\phi}_g(\underline{r})dV$ intersect for a particular value of $1/D_g$. At this value of $1/D_g$, $\int_{V_i} \bar{\phi}_g(\underline{r})dV$ resulting from Eq. (3.32) is identical to $\int_{V_i} \bar{\phi}_g(\underline{r})dV$ computed from Eq. (3.33). It was found that the value of $\int_{V_i} \bar{\phi}_g(\underline{r})dV$ at the intersection is a very good estimate of the true $\int_{V_i} \bar{\phi}_g(\underline{r})dV$ needed in Eq. (1.3). The $\int_{V_i} \bar{\phi}_g(\underline{r})dV$ calculated in this manner has two very satisfying properties: (1) It depends upon the linear functions of both Eq. (3.32) and (3.33). Thus, all available information concerning the surface group fluxes and group currents is used to determine the flux integral;

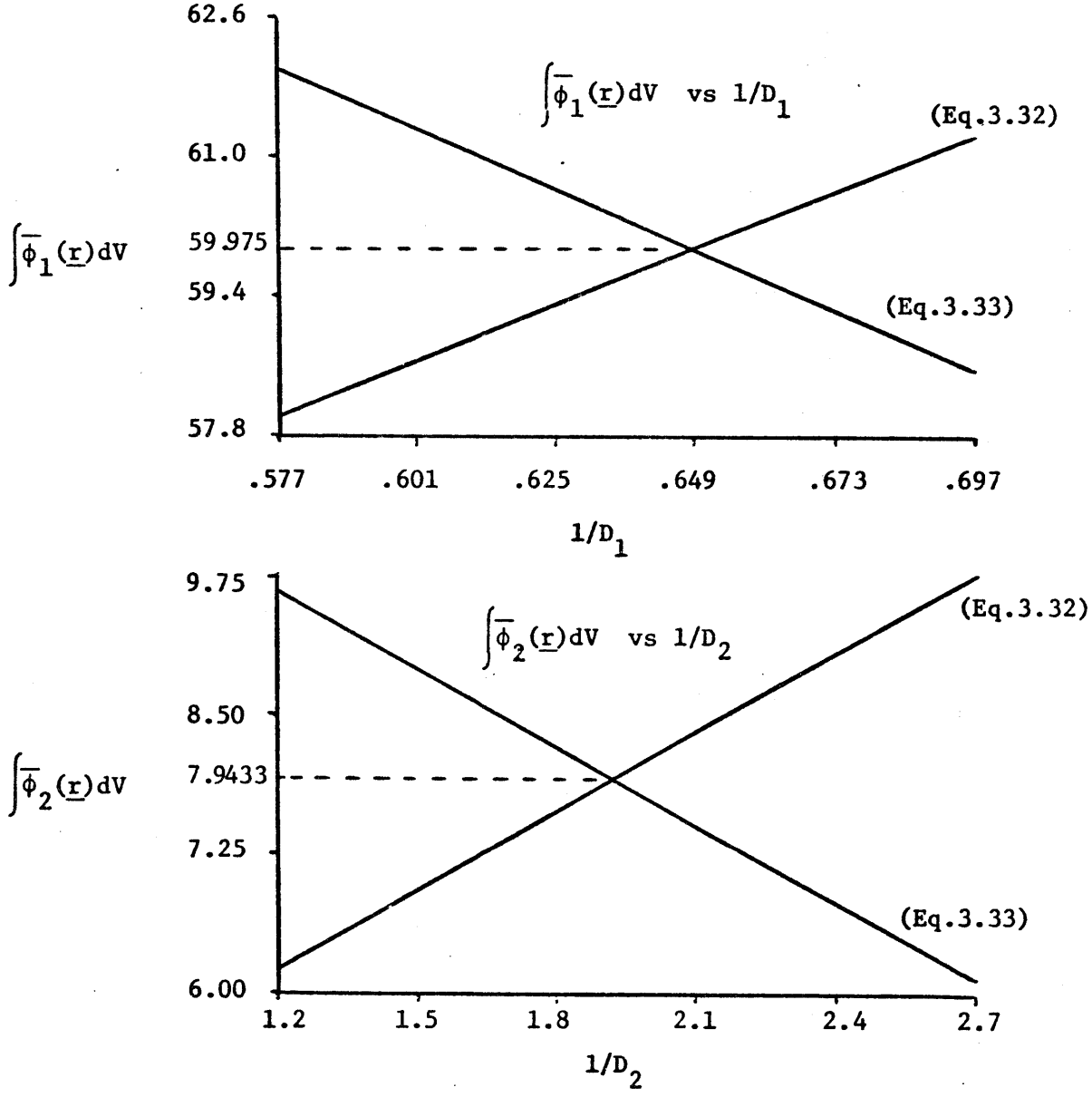

SAMPLE CASE

BWR Assembly A Near Center of Large Number of Like Assemblies

FIGURE 3.6

Linear Curves of the Integrated Homogeneous Flux Shape Resulting from Cubic-Hermite Expansions as a Function of The Inverse of the Diffusion Coefficient

and (2) The value of $1/D_g$ is not required since the value of $\int_{V_i} \bar{\phi}_g(\underline{r})dV$ is computed at the particular value of $1/D_g$ where a plot of the two linear functions intersect. Various other methods of combining Eqs. (3.32) and (3.33) were examined but none proved to be as satisfactory as the above intercept technique.

The value of $\int_{V_i} \bar{\phi}_g(\underline{r})dV$ computed from this intercept technique can be written analytically by eliminating $1/D_g$ from Eqs. (3.32) and (3.33) and solving for $\int_{V_i} \bar{\phi}_g(\underline{r})dV$ such that

$$\int_{V_i} \bar{\phi}_g(\underline{r})dV = (m'_g b_g - m_g b'_g)/(m'_g - m_g) \tag{3.33}$$

where

$$m'_g \equiv \frac{h_y^2}{12}[\tilde{J}^1_g + \tilde{J}^2_g] \tag{3.34a}$$

$$m_g \equiv \frac{h_x^2}{12}[\tilde{J}^4_g + \tilde{J}^3_g] \tag{3.34b}$$

$$b'_g \equiv \frac{h_y}{2}[\tilde{\phi}^1_g + \tilde{\phi}^2_g] \tag{3.34c}$$

$$b_g \equiv \frac{h_x}{2}[\tilde{\phi}^4_g + \tilde{\phi}^3_g] \tag{3.34d}$$

Recall that the $\tilde{J}_g^{\ell}$'s and $\tilde{\phi}_g^{\ell}$'s can be written in terms of the current response matrices of the heterogeneous assembly.

The intercept method was found to give an accurate estimate of $\int_{V_i} \bar{\phi}_g(\underline{r})dV$ for various types of assembly geometries and various assembly boundary conditions. (The $\tilde{\phi}_g^{\ell}$'s and $\tilde{J}_g^{\ell}$'s depend upon the $[J_{in}^{\ell}]_i$'s and $[J_{out}^{\ell}]_i$'s which in turn depend upon assembly placement.) The values are compared to the "true" $\int_{V_i} \bar{\phi}_g(\underline{r})dV$ (which are taken to be the solution of the double-iterative scheme described in Chapter 2) and the results are shown in Table 3.3. Also shown in this table is $\int_{V_i} \phi_g(\underline{r})dV$, the integral of the group flux shape in the heterogeneous assembly. The conventional flux-weighting procedure assumes that $\int_{V_i} \bar{\phi}_g(\underline{r})dV = \int_{V_i} \phi_g(\underline{r})dV$. Note the large errors that result when this approximation is made.

Examination of Table 3.3 reveals that the intercept method gives a good estimate of $\int_{V_i} \bar{\phi}_g(\underline{r})dV$ for all assembly types and all assembly locations. The calculation of the $\bar{\Sigma}_{\alpha g}^{(i)}$'s using the $\int_{V_i} \bar{\phi}_g(\underline{r})dV$ of the Cubic-Hermite-Intercept

TABLE 3.3

Results of the Cubic-Hermite-Intercept Method for Calculating $\int_{V_i} \overline{\phi}(\underline{r})\,dV$*

$$\frac{\int \overline{\phi}_g(\underline{r})\,dV}{}$$

Assembly** Position i	Exact g=1 / g=2	CHI g=1 / g=2	FW*** g=1 / g=2
		BWR Assemblies	
AI	5.9971+1	5.9975+1(.01)	5.9847+1(-.21)
	7.9420+0	7.9433+0(.02)	6.9942+0(-11.93)
BI	4.8776+1	4.8764+1(-.03)	4.8551+1(-.46)
	8.3324+0	8.3226+0(-.12)	9.0146+0(8.19)
Q1	6.1636+1	6.1865+1(.37)	6.1335+1(-.49)
	1.4575+1	1.5121+1(3.75)	1.3286+1(-8.84)
Q2,Q4	1.8324+2	1.8325+2(.01)	1.8230+2(-.51)
	3.7599+1	3.7762+1(.43)	4.0324+1(7.25)
Q3,Q7	1.5696+2	1.5720+2(.15)	1.5642+2(-.34)
	2.8015+1	2.8539+1(1.87)	2.5174+1(-10.14)
Q5,Q9	5.1593+1	5.1616+1(.04)	5.1465+1(-.25)
	7.3924+0	7.3892+0(-.04)	6.5511+0(-11.38)

(continued on next page)

TABLE 3.3 (continued)

$$\int \bar{\phi}_g(\underline{r})\,dV$$

Assembly** Position i	Exact g=1 g=2	CHI g=1 g=2	FW*** g=1 g=2
		BWR Assemblies	
Q6,Q8	5.7892+1	5.7845+1(-.08)	5.7643+1(-.43)
	9.0894+0	9.0972+0(.09)	9.8767+0(8.66)
H1-H7,H9 are identical to Q1-Q7,Q9 (see Table 4.6)			
H8	1.7879+2	1.7868+2(-.06)	1.7800+2(-.44)
	2.8590+1	2.8517+1(-.26)	3.1043+1(8.58)
H10	1.5401+2	1.5402+2(.01)	1.5322+2(-.51)
	3.1510+1	3.1645+1(.43)	3.3797+1(7.26)
H11	5.0865+1	5.0841+1(-.05)	5.0630+1(-.46)
	8.5040+0	8.4985+0(-.06)	9.2118+0(8.32)
H12	1.9100+2	1.9092+2(-.04)	1.9013+2(-.46)
	3.1511+1	3.1442+1(-.22)	3.4158+1(8.40)
H13	3.7293+1	3.7389+1(.26)	3.7067+1(-.61)
	9.9854+0	1.0193+1(2.08)	1.0601+1(6.17)

(continued on next page)

TABLE 3.3 (continued)

$$\int \bar{\phi}_g(\underline{r})\,dV$$

Assembly** Position i	Exact g=1 g=2	CHI g=1 g=2	FW*** g=1 g=2
		BWR Assemblies	
H14,H15	9.9411+1	9.9450+1(.04)	9.8903+1(-.51)
	2.0415+1	2.0534+1(.58)	2.1893+1(7.24)
		PWR Assemblies	
EI	1.0345+2	1.0294+2(-.49)	1.0299+2(-.44)
	2.3272+1	2.3136+1(-.58)	2.5341+1(8.89)
DI	9.2398+1	9.1919+1(-.52)	9.1803+1(-.64)
	2.3285+1	2.3141+1(-.62)	2.5048+1(7.57)
$D^W I$	7.4470+1	7.5002+1(.71)	7.2676+1(-2.41)
	1.6968+1	1.7119+1(.89)	1.5864+1(-6.51)
P1	2.6001+2	2.6089+2(.34)	2.5916+2(-.33)
	4.6739+1	4.6057+1(-1.46)	5.1308+1(9.78)
P2			

*Numbers in parenthesis are per cent difference from exact value.

**Assembly positions refer to Figures (4.1,4.2 and 4.3). Those positions ending in I (AI,EI,etc.) represent the corresponding assembly as if it were surrounded by a large number of like assemblies.

***FW represents $\int_{V_i} \phi_g(\underline{r})dV$, the integral of the flux resulting from the i^{th} cell calculation which would be used in a normal flux-weighting procedure.

method eliminates the need for a double-iterative search since the homogenized cross sections are calculated before the group diffusion coefficients search is performed. In the next section the scheme for determining the $\bar{D}_g$'s is discussed.

3.4 Calculation of the Homogenized Group Diffusion Coefficients

The ideal set of $\bar{D}_g$'s would result in the transmission of neutrons through the homogeneous assembly that would closely match the actual transmission through the heterogeneous assembly. This could best be accomplished if $\bar{D}_g$'s could be found such that their use with the $\bar{\Sigma}_{\alpha g}^{(i)}$'s in the homogeneous cell calculation would result in current response matrix elements identical to those of the heterogeneous assembly. However, a set of $\bar{D}_g$'s cannot be found whose use will match all the response matrix elements.

Several methods for computing the $\bar{D}_g$'s were examined. The values of $\bar{D}_1$ and $\bar{D}_2$ which best describe the "true" neutron transmission of neutrons were those found be requiring that the largest $R_{11}^{\ell\ell'}$ and the largest $R_{22}^{\ell\ell'}$ (ℓ=1,2,3,4; ℓ'=1,1,3,4) of the heterogeneous assembly be reproduced in the homogeneous cell calculation. For example, suppose the largest $R_{11}^{\ell\ell'}$ and $R_{22}^{\ell\ell'}$ of the heterogeneous cell are R_{11}^{31} and R_{22}^{11}. Recall that R_{11}^{31} is the fraction of neutrons entering face one in group one and leaving face three in group one. R_{22}^{11} is the fraction of group two neutrons entering face one

and leaving face one in group two. Initial values of $\bar{D}_1$ and $\bar{D}_2$ are chosen and are used with the $\bar{\Sigma}_{\alpha g}^{(i)}$'s computed using the Cubic-Hermite-Intercept technique in a now homogeneous cell calculation. Note that, since response elements are being matched (in this example R_{11}^{31} and R_{22}^{11}), only the response matrix calculation need be performed. Next, the R_{11}^{31} and R_{22}^{11} resulting from the homogeneous cell calculation are compared to the corresponding elements of the heterogeneous cell calculation. The search continues until the true R_{11}^{31} and R_{22}^{11} are reproduced in the homogeneous assembly.

The search for the proper $\bar{D}_1$ and $\bar{D}_2$ was found to require only several (3 to 7) homogeneous assembly calculations. One reason is that, for fixed cross sections, $R_{11}^{\ell\ell'}$ is largely dependent upon the value of $\bar{D}_1$ and only slightly dependent upon $\bar{D}_2$ since $R_{11}^{\ell\ell'}$ is the fraction of neutrons entering and leaving the assembly in group one. The same is true of the dependence of $R_{22}^{\ell\ell'}$ on $\bar{D}_2$. In addition, for most assemblies the largest $R_{gg}^{\ell\ell'}$'s are the R_{gg}^{11}'s (the group g to group g reflection element), and R_{gg}^{11} is even more dependent upon $\bar{D}_g$ (and not $\bar{D}_{g'}$) than are the other $R_{gg}^{\ell'}$ ($\ell'\neq 1$). (R_{gg}^{11} is the only g to g reflection matrix for a quarter-symmetric assembly. For non-symmetric assemblies there may exist $R_{gg}^{\ell\ell}$ ($\ell\neq 1$) larger than R_{gg}^{11}.) Since the largest $R_{11}^{\ell\ell'}$ to be matched is primarily a function of $\bar{D}_1$ and not $\bar{D}_2$, the effect of the value

of $\bar{D}_1$ upon the resulting value of $R_{11}^{\ell\ell'}$ can be monitored and a new guess of $\bar{D}_1$ is made using linear extrapolation techniques. The same is true for $\bar{D}_2$ in relation to the largest $R_{22}^{\ell\ell'}$. Although there is a slight dependence of $R_{gg}^{\ell\ell'}$ upon $\bar{D}_{g'}$, the above search scheme was found to work quite well for all cases.

Another advantage of matching the largest $R_{11}^{\ell\ell'}$ and $R_{22}^{\ell\ell'}$ is that, for assembly geometries typical of most reactors, these elements are the largest response elements of all the $R_{gg'}^{\ell\ell'}$. Thus, the $\bar{D}_g$'s obtained by matching the largest $R_{gg}^{\ell\ell'}$ guarantee the proper transmission of a large portion of the neutrons. Also, most of the remaining $R_{gg'}^{\ell\ell'}$ elements of the homogeneous assembly are very close in value to the corresponding elements of the heterogeneous assembly. Table 3.4 lists the response matrix elements of the homogeneous and heterogeneous assembly of a typical BWR. Also shown are the values of $\bar{D}_g$ and the D_g found from the conventional flux-weighting technique. Note that the "true" elements R_{11}^{31} and R_{22}^{11} are reproduced in this case. Table 3.5 lists the corresponding information for a typical PWR assembly.

The response matrix calculations are independent of the assembly's boundary conditions. However, $\bar{D}_1$ and $\bar{D}_2$ will be slightly dependent upon the assembly's position in the core since the $\bar{\Sigma}_{\alpha g}^{(i)}$'s used in the homogeneous cell calculation are a function of assembly position i.

TABLE 3.4

Comparison of Response Matrix Elements Resulting From Heterogeneous Cell Calculation and Homogeneous Cell Calculation - BWR*

	Heterogeneous	EGDC
R_{11}^{11}	1.3830-1	1.4024-1
R_{21}^{11}	2.5569-2	2.4174-2
R_{12}^{11}	2.4527-1	2.1374-1
R_{22}^{11}*	3.1761-1	3.1761-1
R_{11}^{21}	1.2050-1	1.2461-1
R_{21}^{21}	5.6685-3	6.4872-3
R_{12}^{21}	5.4377-2	5.7356-2
R_{22}^{21}	5.6696-3	8.2337-3
R_{11}^{31}*	3.3218-1	3.3218-1
R_{21}^{31}	1.2104-2	1.2168-2
R_{12}^{31}	1.1611-1	1.0758-1
R_{22}^{31}	1.2649-1	1.2689-1

(continued on next page)

TABLE 3.4 (continued)

	Diffusion Coefficients	
	Group 1	Group 2
$D^{\text{Flux-weighted}}$	1.3884	.38420
$\overline{D}^{\text{EGDC}}$	1.4093	.38073

*Homogeneous cell calculation uses group diffusion coefficients found by matching largest response matrix elements of heterogeneous cell calculation. Assembly is a BWR type A in an infinite number of like assemblies.

$R_{gg'}^{41}$'s = $R_{gg'}^{31}$'s and are not listed.

TABLE 3.5

Comparison of Response Matrix Elements Resulting from Heterogeneous Cell Calculation and Homogeneous Cell Calculation - PWR*

	Heterogeneous	EGDC
R_{11}^{11}*	3.8942-1	3.8940-1
R_{21}^{11}	6.0189-2	6.2183-2
R_{12}^{11}	4.0448-1	3.9153-1
R_{22}^{11}*	4.2566-1	4.2561-1
R_{11}^{21}	6.0392-2	5.9943-2
R_{21}^{21}	6.6951-3	6.3633-3
R_{12}^{21}	3.9937-2	4.0066-2
R_{22}^{21}	4.4873-3	4.3088-3
R_{11}^{31}	2.3860-1	2.3981-1
R_{21}^{31}	1.9185-2	1.8507-2
R_{12}^{31}	1.1442-1	1.1653-1
R_{22}^{31}	7.6035-2	7.5304-2

(continued on next page)

TABLE 3.5 (continued)

	Diffusion Coefficients	
	Group 1	Group 2
$D^{\text{Flux-weighted}}$	1.4499	.37666
$\bar{D}^{\text{EGDC}}$	1.4458	.40179

*Homogeneous cell calculation uses group diffusion coefficients found by matching largest response matrix elements of heterogeneous cell calculation. Assembly is a PWR type E_{16} in a long strip of different PWR assemblies.

$R^{41}_{gg'}$'s = $R^{31}_{gg'}$'s and are not listed.

Finally, a good initial guess for the $\bar{D}_g$'s can significantly decrease the number of cell calculations required in the search for the proper $\bar{D}_g$'s. If no initial guess is available, flux-weighted values can be calculated from the heterogeneous cell calculation and then used as an initial guess for the $\bar{D}_g$'s.

Although the above scheme for determining the homogenized diffusion coefficients might seem a little like a "cook book" prescription, the technique is quite straightforward, has a plausible theoretical basis, and is easy to program for computer application.

3.5 Summary

The response matrix scheme described in this chapter is an improvement upon the previous scheme. The present scheme results in the two significant improvements that were mentioned as homogenization goals in the introduction to this chapter. Namely, the scheme accounts for assembly position within the reactor and it also decreases the amount of computational effort by eliminating the double-iterative scheme.

A summary of the method is now outlined.

I) Calculate the necessary current response matrices and integrated reaction rate responses for each different assembly composition in a heterogeneous cell calculation.

II) Calculate the albedo matrices for each material composition. For each different assembly composition calculate the $[\alpha^{\ell}]^{k}$'s (ℓ=1,2,3,4) using Eq. (3.26). For quarter-symmetric assemblies the $[\alpha^{\ell}]^{k}$'s are identical for each ℓ and only one $[\alpha^{\ell}]^{k}$ must be computed. The albedo matrices for reflector material can be computed using Kalambokas's[14] expressions.

III) Calculate the $[J_{in}]_i$'s for each assembly position i using Eq. (3.12).

IV) Depending upon assembly symmetry and the values of the $[J_{in}]_i$'s, choose either Eq. (2.6), (3.27a), (3.27b), or (3.27c) as the equation to be used for computing the $\bar{\Sigma}_{\alpha g}$'s of assembly i. Calculate the numerator of the expression for $\bar{\Sigma}_{\alpha g}^{(i)}$ using the integrated reaction rate responses of the heterogeneous assembly. Using the same set of $[J_{in}]_i$'s required in the chosen expression for $\bar{\Sigma}_{\alpha g}^{(i)}$, calculate $\int_{V_i} \bar{\phi}_g(\underline{r})dV$ from Eq. (3.33).

Now compute the $\bar{\Sigma}_{\alpha g}^{(i)}$'s. Repeat this procedure for each assembly position i.

V) Determine the $\bar{D}_g^{(i)}$'s of each assembly position i by the search technique described in Section 3.4.

CHAPTER IV

BWR AND PWR SAMPLE PROBLEMS

4.1 Introduction

The response matrix homogenization technique was used to calculate two-group, two-dimensional equivalent diffusion constants for problems representing geometries typical of boiling and pressurized light water reactors. A description of the sample problems and the results are presented in this chapter.

The BWR problems consist of a reactor core of twenty-five assemblies arranged in a 5 x 5 array. All assemblies in the BWR problems are one of the two assembly types shown in Fig. 2.1. A water reflector surrounds the core. The two-group cross sections and diffusion coefficients for the assembly materials and water reflector are listed in Appendix C.

Two sample BWR problems were examined. The first problem consists of a reactor geometry in which the two different assembly compositions are arranged in a checkerboard array. The reactor has quarter-core symmetry and a description of the resulting quarter-core problem is shown in Fig. 4.1. This problem is identical to the sample problem used in the examination of the previous response matrix scheme (the results of which are shown in Fig. 2.2), and will therefore provide a comparison between the two schemes. Each assembly

position is numbered for later reference, and each assembly composition is identified by either an A or B which represents the corresponding assembly composition shown in Figure 2.1.

The second BWR problem has half-core symmetry, and the resulting half-core problem is shown in Fig. 4.2. Again the assembly positions are numbered and the assembly compositions are represented in the same manner as before.

The choice of a representative PWR problem was governed by practical considerations. The assembly geometries used in the PWR sample problem are those representative of the types used by Combustion Engineering[15] and are shown in Fig. 3.4. It was found that at least two mesh points per fuel (or control, shim, etc.) cell were required for an accurate solution of the heterogeneous benchmark problem and the response matrix cell calculation. Because of the size of the PWR assemblies (i.e. the large number of fuel, control, and shim cells) a realistic quarter-core problem would be prohibitively expensive. In addition the PWR assemblies are more homogeneous in nature than the BWR assemblies. Thus one would expect that the homogenization scheme would be more severly tested by the BWR problems. For this reason the examination of PWR problems with core geometries similar to those of the BWR problems was felt to be unduly repetitious. Nevertheless some test of the present scheme's applicability

to PWR geometries was needed. A PWR sample problem using realistic PWR assembly compositions, but not prohibitively expensive and not repetitious with regard to the BWR problems, was chosen and is shown in Fig. 4.3. The nuclear data for the assembly materials, water reflector, and core shroud are given in Appendix C.

4.2 Calculated Data for Sample Problems

The first step of the present homogenization scheme is to calculate the current and integrated reaction rate response matrices for each different assembly composition in the reactor. The response matrices for the BWR assembly compositions are listed in Table 4.1. The notation of assembly types refers to the assemblies shown in Fig. 2.1. The response matrices of the PWR assembly compositions are listed in Table 4.2 and the assembly types refer to those shown in Fig. 3.4. Note that all assemblies, both BWR and PWR, are quarter-symmetric and only the response matrices for neutrons incident upon one face were calculated.

The second step in the homogenization technique requires that the albedo matrices of each assembly composition (and reflector material, etc.), the $[\alpha^{\ell}]^{k}$'s, be determined using Eq. (3.26) for assembly compositions and Kalambokas's results[14] for reflector material. The material albedo matrices for the BWR and PWR assemblies were calculated and are listed in Tables 3.1 and 3.2 respectively. Since all

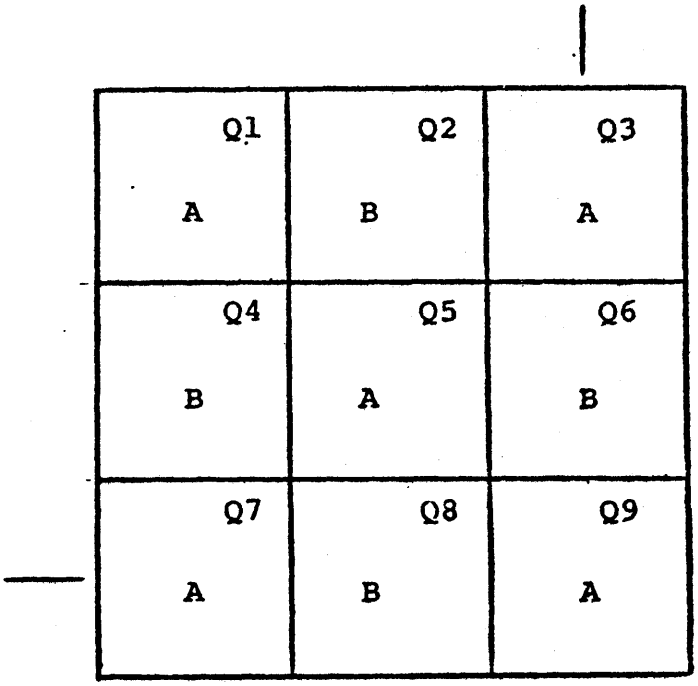

Assembly types A and B refer to the assemblies shown in Figure 2.1.

Numbers in upper right hand corner represent assembly position.

An eight cm water reflector surrounds the core.

Mesh Spacing

Heterogeneous reference problem: 5 cm spacing throughout core and reflector

Homogeneous problems: 5 cm in reflector and fuel within 2 cm of interface and 1 cm elsewhere

FIGURE 4.1

BWR Quarter-Core Configuration

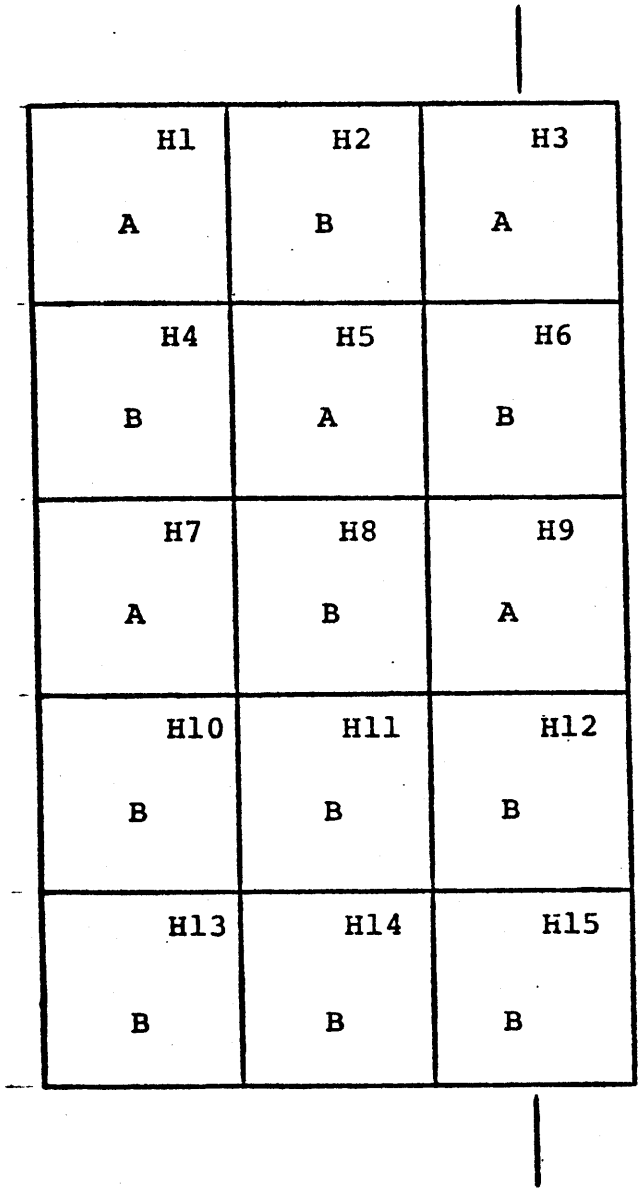

Assembly types A and B refer to the assemblies shown in Figure 2.1.
Numbers in upper right hand corner represent assembly position.
An eight cm water reflector surrounds the core.

Mesh spacing for heterogeneous and homogeneous problems corresponds to that used for quarter-core problems.

FIGURE 4.2

BWR Half-Core Configuration

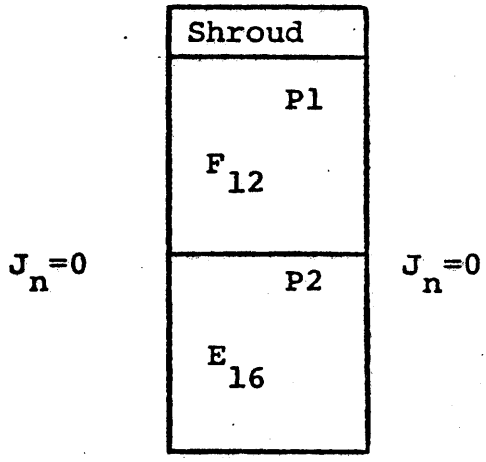

Assemblies F_{12} and E_{16} refer to those shown in Figure 3.4.

Number in upper right corner refers to assembly position.

The shroud is 2.59715 cm in thickness, and there is zero net leakage out of the sides of the strip.

There is a 20.6248 cm water reflector on the outside of the shroud.

The mesh spacing is .7366 cm for all problems.

FIGURE 4.3

PWR Strip Configuration

TABLE 4.1

Response Matrices of Heterogeneous Assembly BWR Compositions*

	Assembly A	Assembly B
R_{11}^{11}	1.3830-1	1.3475-1
R_{21}^{11}	2.5569-2	2.9758-2
R_{12}^{11}	2.4527-1	2.6099-1
R_{22}^{11}	3.1761-1	3.3033-1
R_{11}^{21}	1.2050-1	1.2937-1
R_{21}^{21}	5.6685-3	9.3373-3
R_{12}^{21}	5.4377-2	7.0244-2
R_{22}^{21}	5.6696-3	1.2291-2
R_{11}^{31}	3.3218-1	3.3574-1
R_{21}^{31}	1.2104-2	1.5989-2
R_{12}^{31}	1.1611-1	1.3189-1
R_{22}^{31}	1.2649-1	1.3534-1

*$R_{gg'}^{41}$'s = $R_{gg'}^{31}$'s and are not listed. Assemblies refer to those shown in Figure 2.1.

TABLE 4.2

Response Matrices of Heterogeneous Assembly PWR Compositions*

	Assembly F_{12}	Assembly E_{16}	Assembly D_0	Assembly D_0^W
R_{11}^{11}	3.9426-1	3.8942-1	3.8768-1	3.4476-1
R_{21}^{11}	5.2409-2	6.0189-2	6.3575-2	5.2183-2
R_{12}^{11}	4.2684-1	4.0448-1	3.6300-1	3.1988-1
R_{22}^{11}	3.9024-1	4.2566-1	4.4870-1	4.3078-1
R_{11}^{21}	5.9761-2	6.0392-2	5.9412-2	3.4443-2
R_{21}^{21}	5.2588-3	6.6951-3	7.1293-3	3.2800-3
R_{12}^{21}	3.7864-2	3.9937-2	3.6986-2	1.9344-2
R_{22}^{21}	3.3563-3	4.4873-3	4.5198-3	1.8831-3
R_{11}^{31}	2.3898-1	2.3860-1	2.3793-1	1.9990-1
R_{21}^{31}	1.5675-2	1.9185-2	2.0252-2	1.2862-2
R_{12}^{31}	1.1305-1	1.1442-1	1.0635-1	7.6324-2
R_{22}^{31}	6.7817-2	7.6035-2	7.7202-2	6.9468-2

*$R_{gg'}^{41}$'s = $R_{gg'}^{31}$'s and are not listed. Assemblies refer to those shown in Figure 3.4.

assemblies are quarter-symmetric, only the $[\alpha^{l}]^{k}$'s were computed. The positional albedoes matrices associated with assembly i used in Eq. (3.11), the $[\alpha^{\ell}]_i$'s, are the $[\alpha^{\ell}]^{k}$'s of the adjacent material k. The $[\alpha^{\ell}]_i$'s of each position i for both the BWR and PWR sample problems are listed in Appendix C.

Once the $[\alpha^{\ell}]_i$'s were determined, the $[J_{in}]_i$'s were calculated for each position i using Eq. (3.12). The incoming partial current matrices for the BWR quarter-core assembly positions shown in Fig. 4.1 were computed and are listed in Table 4.3. The $[J_{in}]_i$'s for the BWR half-core problem (Fig. 4.2) are given in Table 4.4. The incoming group partial currents for the assemblies comprising the PWR sample problem shown in Fig. 4.3 are listed in Table 4.5.

The $[J_{in}]_i$'s having been obtained for each assembly position i, the cross sections were computed using the Cubic-Hermite expressions for $\int_{V_i} \bar{\phi}_g(\underline{r})dV$ given by Eq. (3.33)

in conjunction with the appropriate equation (3.27a, 3.27b, or 3.27c) defining $\bar{\Sigma}^{(i)}_{\alpha g}$. The diffusion coefficients were then determined by the technique outlined in Chapter 4. An interesting point is that, during the process of performing the homogeneous cell calculation for determining the $\bar{D}_g$'s, the actual $\int_{V_i} \bar{\phi}_g(\underline{r})dV$ can be calculated and $\bar{\Sigma}^{(i)}_{\alpha g}$

TABLE 4.3

Incoming Group Partial Currents

BWR Quarter-Core Problem*

Position i**	$J_1^1(in,i)$ / $J_2^1(in,i)$	$J_1^2(in,i)$ / $J_2^2(in,i)$	$J_1^3(in,i)$ / $J_2^3(in,i)$	$J_1^4(in,i)$ / $J_2^4(in,i)$
Q1	5.6884	--	--	1.4469
	1.0000	--	--	1.6220
Q2,Q4	6.8796	2.1842	6.3237	6.3237
	1.0000	2.2347	.99397	.99397
Q3,Q7	6.2291	1.6551	5.5712	5.5712
	1.0000	1.5429	.93514	.93514
Q5,Q9	6.4247	--	--	--
	1.0000	--	--	--
Q6,Q8	7.1336	--	--	--
	1.0000	--	--	--

*Partial currents are those used in Eq. (3.27a,b or c). Notation for partial currents refers to Figure 3.2.

**Assembly position refers to Figure 4.1.

TABLE 4.4

Incoming Group Partial Currents

BWR Half-Core Problem*

Assembly Position i**	$J_1^1(in,i)$ $J_2^1(in,i)$	$J_1^2(in,i)$ $J_2^2(in,i)$	$J_1^3(in,i)$ $J_2^3(in,i)$	$J_1^4(in,i)$ $J_2^4(in,i)$
H1-H7, H9 are identical to Q1-Q7,Q9 (see Table 4.3)				
H8	6.1729 1.0000	5.1581 .71801	5.3232 .74665	5.3232 .74665
H10	5.7198 1.0000	4.7508 .73115	6.1583 1.0228	1.6278 1.6142
H11	6.2156 1.0000	-- --	-- --	-- --
H12	6.1827 1.0000	5.1791 .72213	6.0097 .96736	6.0097 .96736
H13	.84656 1.0000	-- --	3.3433 .60638	-- --
H14,H15	1.0151 1.0000	3.8396 .63628	3.4613 .60045	3.4613 .60045

*Partial currents are those used in Eqs. (3.27a,b or c). Notation for partial currents refers to Figure 3.2.

**Assembly position refers to Figure 4.2.

TABLE 4.5

Incoming Group Partial Currents

PWR Problem*

Position i**	$J_1^1(in,i)$	$J_1^2(in,i)$	$J_1^3(in,i)$	$J_1^4(in,i)$
	$J_2^1(in,i)$	$J_2^2(in,i)$	$J_2^3(in,i)$	$J_2^4(in,i)$
P1	5.2234	1.0683	2.7870	2.7870
	1.0000	.26411	.47269	.47269
P2	8.5725	23.672	15.183	15.183
	1.0000	4.0388	3.0817	3.0817

*Partial currents are those used in Eq. (3.27a,b or c). Notation for partial currents refers to Figure 3.2.

**Assembly position refers to Figure 4.3.

can be recalculated using this value. Since the initial Cubic-Hermite estimate of $\int_{V_i} \bar{\phi}_g(\underline{r})dV$ is very accurate, the $\bar{\Sigma}_{\alpha g}^{(i)}$'s change very little and recalculating them does not interfere with the linear extrapolation scheme for determining the $\bar{D}_g$'s. The cross sections used for the sample problems were calculated in this manner.

The two-group cross sections and diffusion coefficients for the assemblies comprising the BWR quarter-core reactor problem are listed in Table 4.6. Note that they are positionally dependent; the assembly position notation refers to Fig. 4.1. The conventional FWC of each assembly composition is also given in Table 4.6. The EGDC and FWC calculated for the assemblies of the half-core BWR problem described in Fig. 4.2 are listed in Table 4.7. The homogenized diffusion constants for the PWR problem are given in Table 4.8 where the notation for assembly position refers to the assemblies shown in Fig. 4.3.

4.3 BWR Results

A quarter-core criticality calculation was performed for the fine-mesh heterogeneous reactor geometry of the quarter-core BWR problem depicted in Fig. 4.1. Two criticality calculations were then performed for the reactor consisting of homogenized assemblies with the EGDC and FWC listed in Table 4.6. The resulting per cent errors in

TABLE 4.6

Diffusion Theory Parameters - FWC and EGDC

BWR Quarter-Core Problem

EGDC

Position i*	$\overline{D}_1$ / $\overline{D}_2$	$\overline{\Sigma}_{a1}$ / $\overline{\Sigma}_{a2}$	$\overline{\nu\Sigma}_{f1}$ / $\overline{\nu\Sigma}_{f2}$	$\overline{\Sigma}_{21}$ / --
Q1	1.4227+0	9.6577-3	6.4599-3	1.4137-2
	3.7917-1	1.0887-1	1.3137-1	--
Q2,Q4	1.4418+0	9.3628-3	6.4635-3	1.7228-2
	3.9236-1	9.6631-2	1.4356-1	--
Q3,Q7	1.4209+0	9.6759-3	6.4735-3	1.4167-2
	3.7991-1	1.0843-1	1.2886-1	--
Q5,Q9	1.4193+0	9.6880-3	6.4824-3	1.4186-2
	3.8037-1	1.0814-1	1.2654-1	--
Q6,Q8	1.4414+0	9.3766-3	6.4732-3	1.7234-2
	3.9252-1	9.6530-2	1.4319-1	--

FWC

Assembly A	1.3884+0	9.7122-3	6.4987-3	1.4222-2
	3.8420-1	1.2155-1	1.4303-1	--
Assembly B	1.4470+0	9.4224-3	6.5050-3	1.7302-2
	3.7478-1	8.9222-2	1.3241-1	--

*Assembly position refers to Figure 4.1.

TABLE 4.7

Diffusion Theory Parameters - FWC and EGDC

BWR Half-Core Problem

EGDC

Position i*	$\overline{D}_1$ $\overline{D}_2$	$\overline{\Sigma}_{a1}$ $\overline{\Sigma}_{a2}$	$\overline{\nu\Sigma}_{f1}$ $\overline{\nu\Sigma}_{f2}$	$\overline{\Sigma}_{21}$ --
H1-H7,H9 are identical to Q1-Q7,Q9 (Table 4.6)				
H8	1.4415+0	9.3745-3	6.4717-3	1.7231-2
	3.9246-1	9.6568-2	1.4326-1	--
H10	1.4418+0	9.3629-3	6.4636-3	1.7228-2
	3.9236-1	9.6631-2	1.4355-1	--
H11	1.4416+0	9.3724-3	6.4703-3	1.7230-2
	3.9242-1	9.6584-2	1.4332-1	---
H12	1.4415+0	9.3731-3	6.4708-3	1.7231-2
	3.9243-1	9.6579-2	1.4330-1	---
H13	1.4420+0	9.3466-3	6.4520-3	1.7222-2
	3.9220-1	9.6695-2	1.4382-1	---
H14,H15	1.4418+0	9.3628-3	6.4635-3	1.7228-2
	3.9234-1	9.6632-2	1.4356-1	---

FWC

FWC for Assembly A and B are same as those for BWR Quarter-Core Problem given in Table 4.6.

*Assembly position refers to Figure 4.2.

TABLE 4.8

Diffusion Theory Parameters - FWC and EGDC

PWR Problem

Position i*	$\bar{D}_1$	$\bar{\Sigma}_{a1}$	$\overline{\nu\Sigma}_{f1}$	$\bar{\Sigma}_{21}$
	$\bar{D}_2$	$\bar{\Sigma}_{a2}$	$\overline{\nu\Sigma}_{f2}$	--
EGDC				
P1	1.4706+0	8.8855-3	5.7202-3	1.7288-2
	3.8559-1	9.2418-2	1.2507-1	---
P2	1.4373+0	9.1954-3	5.1427-3	1.7557-2
	4.0809-1	7.3768-2	1.0848-1	---
FWC				
Assembly F_{12}	1.4462+0	8.8782-3	5.7184-3	1.7224-2
	3.7264-1	8.4492-2	1.1493-1	---
Assembly E_{16}	1.4499+0	9.2048-3	5.1507-3	1.7531-2
	3.7666-1	6.7498-2	9.8895-2	---

*Assembly position refers to Figure 4.3.

assembly powers and reactor K_{eff} are shown in Fig. 4.4. All criticality calculations were normalized to the same total reactor power. The mesh layout for both the heterogeneous and homogeneous problems is shown in Fig. 4.1.

The use of EGDC for the half-core BWR problem depicted in Fig. 4.2 was examined in a similar manner. A criticality calculation was performed for the fine-mesh heterogeneous reactor geometry and for the homogeneous reactor geometries using the EGDC and FWC given in Table 4.7. The per cent errors in assembly powers and reactor K_{eff} are shown in Fig. 4.5. Note that the assembly compositions comprising one portion of the core in this problem represent assemblies in which the cross-shaped control rod has been withdrawn. The resulting flux distribution is tilted towards one side of the reactor. This is an important point because the results of this half-core problem illustrate the applicability of EGDC for reactor conditions in which significant flux tilting may occur.

4.4 PWR Results

The PWR problem depicted in Fig. 4.3 consists of two assemblies, a shroud and water reflector at one end of this short strip, and albedo boundary conditions at the opposite end. This problem is designed to represent the reactor conditions present in two assemblies along the centerline of a half-core symmetric reactor and near the reflector.

XX	Per cent error in Power - FWC
XX	Per cent error in Power - EGDC

Q1 1.74 - .25	Q2 -3.88 .48	Q3 3.67 - .68
	Q5 5.63 - .47	Q6 -3.18 .42
		Q9 5.18 - .63

	FWC	EGDC
Per cent error in K_{eff}	-.847	-.379

FIGURE 4.4

BWR Quarter-Core Results

.XX	Reference per cent total power
XX	Per cent error in power - FWC
XX	Per cent error in power - EGDC

H1	H2	H3
2.288	3.257	3.025
1.02	-4.57	2.83
- .74	.03	-1.18
H4	**H5**	**H6**
3.426	3.393	4.424
-4.33	5.08	-3.64
.15	- .84	.14
H7	**H8**	**H9**
3.448	4.906	4.473
3.76	-2.16	6.29
- .97	.32	- .64
H10	**H11**	**H12**
4.238	5.164	5.593
-1.39	.80	.39
.17	.60	.75
H13	**H14**	**H15**
3.841	4.699	5.167
-1.03	.25	.36
- .05	.38	.41

	Reference	FWC per cent error	EGDC per cent error
K_{eff}	.842530	-.572	-.197

FIGURE 4.5

BWR Half-Core Results

The heterogeneous, fine-mesh solution was first obtained from a criticality calculation. The homogeneous assemblies with the EGDC and FWC listed in Table 4.8 were then used in two criticality calculations respectively. The mesh layout for each problem is shown in Fig. 4.3. The total power in the strip was normalized to the same value for all problems. The resulting per cent errors in assembly powers and K_{eff} of the strip are shown in Fig. 4.6.

An important point to recognize is that the boundary conditions of this short strip are close to being zero current along each edge of both assemblies. Thus, since the FWC are found for exactly these conditions, their use in this problem should lead to accurate results; that they do is evident from Fig. 4.6. The applicability of the present scheme for computing EGDC for PWR assembly geometries is also evident.

A discussion of the sample problem in this chapter and recommendations for future study are presented in the following chapter.

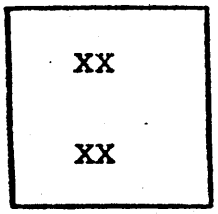

Per cent error in power - FWC

Per cent error in power - EGDC

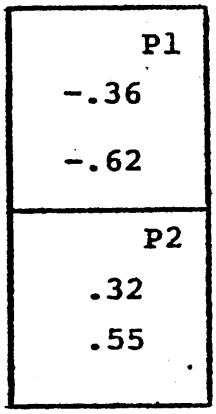

	FWC	EGDC
Per cent error in K_{eff}	-.098	.024

FIGURE 4.6

PWR Strip Results

CHAPTER V

DISCUSSION OF RESULTS AND RECOMMENDATIONS FOR FUTURE STUDY

5.1 Discussion of Results

The use of the response matrix scheme for determining two-group, two-dimensional equivalent diffusion theory parameters results in an accurate prediction of the neutron behavior for both BWR and PWR reactor geometries. The magnitude of the per cent error in assembly power is small (<1.18%) for all sample problems. In addition, the per cent error in reactor K_{eff} (a measure of overall reactor behavior) is less than 0.4% for all problems. The results shown in Chapter 4 indicate that the use of conventional FWC does not result in such an accurate prediction of neutron behavior, but instead leads to significant per cent errors in assembly powers.

The results of the quarter-core BWR problem are shown in Fig. 4.4. The magnitude of the per cent errors in assembly powers when the EGDC are used is less than one per cent for all assemblies, the largest being -.68%. The use of FWC, however, results in assembly powers that are all at least one per cent in error; the per cent errors in fact range from 1.74% to 5.81%. Also the value of K_{eff} calculated using the EGDC is more accurate than that resulting from the use of FWC (-.393% error compared to -.847%). These large differences in per cent errors in

assembly powers and K_{eff} resulting from the use of FWC as compared to EGDC indicate the stronger theoretical foundation of the response matrix homogenization approach over the conventional flux-weighting procedure.

Recall also that the previous method of calculating EGDC by a response matrix approach (see Chapter 2) was tested using this same problem, the results of which are shown in Fig. 2.2. Comparison of Figs. 2.2 and 4.4 indicate the improvement of the present homogenization scheme over the previous technique. The per cent errors in the powers for assemblies bordering the reflector are much lower as a result of using the albedo boundary conditions for calculating the relative partial group currents entering each face of an assembly. Previously it was assumed that each assembly, even those adjacent to the reflector, was near the center of a large array of like assemblies. The theoretical improvement of accounting for assembly position within the reactor is obvious. Now all the assembly power per cent errors are less than one per cent compared to a high of -3.39% using the EGDC found by the previous response matrix technique. In addition, the magnitude of the per cent error in K_{eff} dropped from -.809% to -.397%.

The results of the half-core BWR problem are shown in Fig. 4.5. Again the use of EGDC is an improvement upon the use of FWC. The largest magnitude of the per cent error in

assembly power is 1.18% using EGDC as compared to a maximum of 6.29% using FWC. For the problem using EGDC, the remaining assembly power per cent errors are all less than one per cent. The corresponding per cent errors for the FWC problem, however, are greater than one per cent over most of the core. The reactor K_{eff} is also predicted more accurately using EGDC.

Note that there is a flux tilt from one side of the core to the other resulting from the withdrawal of the cross-shaped control rods over one portion of the core. The results of this half-core problem demonstrate the applicability of the use of EGDC for situations in which a flux tilt may occur. In particular, the results shown in Fig. 4.5 reveal that the determination of group diffusion coefficients by matching the largest response matrix elements leads to an accurate representation of the "true" transmission of neutrons.

The PWR results, shown in Fig. 4.6, indicate that both the use of EGDC and FWC lead to an accurate prediction of assembly powers for this particular problem. However, the group partial currents entering each assembly as calculated from the homogeneous problem using EGDC are very close in value to the corresponding partial currents resulting from the heterogeneous problem; these partial currents resulting from the homogeneous problem using FWC, however, are not close in value to the heterogeneous results.

Thus the "true" transmission of neutrons is better described when the EGDC are used, and for a larger problem this would be crucial.

In addition, studies indicate that the use of a finer mesh size for the two-assembly problems and for the cell calculations would result in a convergence in the results of the heterogeneous and EGDC problems but not for the heterogeneous and FWC problems. But all assembly power per cent errors shown in Fig. 4.6 are very small and the use of either FWC or EGDC leads to accurate results for this problem. Most importantly, this problem reveals that the present response matrix scheme for calculating EGDC can be applied successfully to PWR geometries.

The evaluation of all group diffusion parameters, both for BWR and PWR geometries, is performed using the same method for all reactor positions. This is an asthetically pleasing property of the homogeneization scheme since the procedure can be easily programmed to account for assembly position by "scanning" an assembly's adjacent material and then using a given subroutine for calculating the EGDC.

An alternate scheme would be to redefine the basic response matrix cell calculation such that it would include the appropriate boundary conditions for a particular assembly position within the reactor. This technique was tried with some degree of success, but it is conceptually inferior to the present scheme in that the homogenization

procedure varies from one assembly position to another. Therefore this alternate scheme was discarded.

The use of the Cubic-Hermite expansions for calculating $\int_{V_i} \bar{\phi}_g(\underline{r})\,dV$ proved quite successful. The Cubic-Hermite estimate is very accurate (see Table 3.3), and by eliminating the double-iterative search used in the previous technique, it substantially reduces the amount of computational effort required. Even with this improvement the calculation of the EGDC for a given assembly location requires more computational effort than does the calculation of the corresponding FWC. However the amount of computer time required to calculate the conventional FWC is quite small in the first place, and the increase in cost to compute the EGDC for a given assembly by the present homogenization scheme is inconsequential.

There is also an increase in homogenization cost as a result of calculating EGDC for each assembly position. But the resulting increase in accuracy is evident. Figs. 2.2 and 4.4 show the results for the same BWR problem, one in which the EGDC depend upon assembly position and the other in which they do not. A comparision of these two figures clearly indicates that there is a substantial improvement in accuracy when positionally dependent EGDC are used. The cost of calculating positionally dependent EGDC and solving the resulting reactor problem is small in

comparison to solving the corresponding heterogeneous, full-core problem. Because the resulting increase in accuracy is significant, the use of positionally dependent EGDC seems warranted.

The two general goals of this thesis were to improve upon the accuracy of the previous response matrix homogenization scheme and at the same time reduce the computational costs. The present homogenization technique accomplished these two goals. In addition, (like the earlier scheme) it is applicable to more than two energy groups and has the theoretically appealing property of reducing to the more exact homogenization procedure for one-dimensional problems.

5.2 Recommmendations for Future Study

The application of EGDC to practical reactor situations seems promising in light of the observations made. Additional specific areas for future study would be:

1) A further study of the scheme for determining the group diffusion coefficients. In particular a method is needed for providing an accurate estimate of the first guess of the diffusion coefficients for the iterative search.
2) An effort to provide a comprehensive, fast running computer code to calculate the EGDC.

Efforts were made during the development of the present scheme to reduce the required amount of computational effort to a minimum. However, no effort was made in this thesis to minimize the computer cost of determining the EGDC since those costs were very small in the first place. Presently the codes used during the calculation of the EGDC are limited in scope and provide information useful in the development of the present scheme but unnecessary in regard to the final technqiue chosen. The combination of these codes into one code would reduce the computer costs significantly.

More general areas of possible study would be:

1) A study of the present scheme for a broader range of time-independent, two-dimensional sample problems. This would include analysis of two-dimensional problems with more than two energy groups.
2) The use of EGDC for time-dependent problems. The first part of the analysis should include a study of Kollas's "exact" EGDC for one-dimensional transient problems. The extension to two-dimensional geometry using the present scheme could then be attempted in view of the 1-D results.

REFERENCES

1. Bell, G.I., and Glasstone, S. 1970. Nuclear Reactor Theory (New York: Van Nostrand Reinhold).

2. Henry, A.F., 1975. Nuclear Reactor Analysis (Cambridge, Mass: The MIT Press).

3. Galanin, A.D., 1962. "The Theory of a Heterogeneous Reactor with Cylindrical Fuel Elements of Finite Radius", J. Nucl. En., 16: 547.

4. Lamarsh, J.R., 1966. Introduction to Nuclear Reactor Theory (Reading, Mass.: Addison-Wesley), Chapter 10.

5. Henry, A.F., 1957. U.S.A.E.C. Report TlD-7532, Part 1, p. 3.

6. Bennewitz, F., Finnemann, H. and Modaschl, H., 1975. "Solution of the Multidimensional Neutron Diffusion Equation by Nodal Expansion", Proc. Conf. on Computational Methods in Nuclear Engineering, CONF-750413, I-99.

7. Deppe, L.O., and Hansen, K.F., 1974. "Application of the Finite Element Method to Two-Dimensional Diffusion Problems", NSE: 54, 456-465.

8. Kang, C.M., and Hansen, K.F., 1973. "Finite Element Methods for Reactor Analysis", NSE: 51, 456-495.

9. Kollas, J.G., 1974. An Investigation of the Equivalent Diffusion Theory Constants Method and the Response Matrix Method for Criticality Calculations (MIT, Ph.D. Thesis, Department of Nuclear Engineering.)

10. Henry, A.F., and Worley, B.A., 1975. "Determination of Equivalent Diffusion Theory Parameters", EPRI Research Report 305.

11. Shimizu, A., 1963. "Response Matrix Method", J. At. Energy Soc. Japan, 5: 359.

12. Shimizu, A., and Aoki, K., 1972. Application of Invariant-Embedding to Reactor Physics (New York, N.Y.: Academic Press).

13. Varga, R.S., 1962. Matrix Iterative Analysis, Prentice-Hall, Englewood Cliffs, N.J.

14. Kalambokas, P.C., and Henry, A.F., November 1975. "The Replacement of Reflectors by Albedo-Type Boundary Conditions", MITNE-183, MIT Department of Nuclear Engineering, Cambridge, Mass.

15. Maine Yankee FSAR.

APPENDIX A

Calculation of the Incoming Group One to Group Two Ratio for the Semi-Infinite Medium Approximation Using an Albedo Boundary Approach

We wish to show that equating each $[\alpha^{\ell}]_i$ of assembly i to the G x G identity matrix and solving Eqs. (3.11) and (3.12) in terms of the response matrices results in an expression for X, the incoming group one to group two partial current ratio, identifcal to Eq. (2.9).

For each $[\alpha^{\ell}]_i$ equal to a two by two identity matrix, $[W]_i$ defined by Eq. (3.11), becomes

$$[W]_i = [R]_i \quad . \tag{C.1}$$

Thus, Eq. (3.12) ($\gamma[J_{in}]_i=[W]_i[J_{in}]_i$) for this case results in the following four matrix equations:

$$\gamma[J^1_{in}]_i=[R^{11}]_i[J^1_{in}]_i+[R^{12}]_i[J^2_{in}]_i+[R^{13}]_i[J^3_{in}]_i+$$

$$[R^{14}]_i[J^4_{in}]_i \tag{C.2a}$$

$$\gamma[J^2_{in}]_i=[R^{21}]_i[J^1_{in}]_i+[R^{22}]_i[J^2_{in}]_i+[R^{23}]_i[J^3_{in}]_i+$$

$$[R^{24}]_i[J^4_{in}]_i \tag{C.2b}$$

$$\gamma[J^3_{in}]_i=[R^{31}]_i[J^1_{in}]_i+[R^{32}]_i[J^2_{in}]_i+[R^{33}]_i[J^3_{in}]_i+$$

$$[R^{34}]_i[J^4_{in}]_i \qquad \text{(C.2c)}$$

$$\gamma[J^4_{in}]_i=[R^{41}]_i[J^1_{in}]_i+[R^{42}]_i[J^2_{in}]_i+[R^{43}]_i[J^3_{in}]_i+$$

$$[R^{44}]_i[J^4_{in}]_i \ . \qquad \text{(C.2d)}$$

Because the assembly i is assumed to be quarter-symmetric, $[R^{\ell\ell'}]_i=[R^{\ell'\ell}]_i$ for all ℓ and ℓ'. In addition, because the assembly is symmetric and because identical boundary conditions are imposed upon each side of the assembly, $[J^{\ell}_{in}]_i$ will be identical for each ℓ. Therefore, the above four equations are redundant and can be written as the following single equation:

$$\gamma[J^1_{in}]_i=\left[[R^{11}]_i+[R^{21}]_i+[R^{31}]_i+[R^{41}]_i\right][J^1_{in}]_i \ . \qquad \text{(C.3)}$$

We now define $C_{gg'}$ such that

$$C_{gg'} \equiv \sum_{\ell'=1}^{4} R^{\ell'1}_{gg'} \qquad \text{(C.4)}$$

where $C_{gg'}$ is defined in the same manner as the C_{gg}, in Eq. (2.9).

The above equation can be written as

$$\gamma[J^1_{in}]_i = \begin{bmatrix} C_{11} & C_{12} \\ C_{21} & C_{22} \end{bmatrix} [J^1_{in}]_i . \qquad (C.5)$$

Solving for the eigenvalue γ results in the quadratic equation

$$\gamma^2 - (C_{11}+C_{22})\gamma + (C_{11}C_{22} - C_{21}C_{12}) = 0 \quad . \qquad (C.6)$$

The solution for the positive root of γ gives

$$\gamma = \frac{(C_{11}+C_{22}) + \sqrt{(C_{11}-C_{22})^2 + 4C_{21}C_{12}}}{2} \quad . \qquad (C.7)$$

Substitution of γ from Eq. (C.7) into the second equation in (C.5) results in the following value of J_1/J_2:

$$J_1/J_2 = X = \frac{C_{11}-C_{22} + \sqrt{(C_{22}-C_{11})^2 + 4C_{12}C_{21}}}{2C_{21}} \quad . \qquad (C.8)$$

Eq. (C.8) is identical to Eq. (2.9).

APPENDIX B

Cubic Hermite Basis Functions

The Cubic Hermite basis functions used in Eqs. (3.30) and (3.31) are defined as follows:

$$u_0^{0+}(x) \equiv [-2(1-x/h_x)^3+3(1-x/h_x)^2]$$

$$u_{h_x}^{0-}(x) \equiv [-2(x/h_x)^3+3(x/h_x)^2]$$

$$u_0^{1+}(x) \equiv [-(1-x/h_x)^3+(1-x/h_x)^2]hx$$

$$u_{h_x}^{1-}(x) \equiv [(x/h_x)^3-(x/h_x)^2]hx$$

$$w_0^{0+}(y) \equiv [-2(1-y/h_y)^3+3(1-y/h_y)^2]$$

$$w_{h_y}^{0-}(y) \equiv [-2(y/h_y)^3+3(y/h_y)^2]$$

$$w_0^{1+}(y) \equiv [-(1-y/h_y)^3+(1-y/h_y)^2]hy$$

$$w_{h_y}^{1-}(y) \equiv [(y/h_y)^3-(y/h_y)2]hy$$

APPENDIX C

DATA FOR BWR AND PWR SAMPLE PROBLEMS

This appendix contains useful information for the sample problems presented in the text of this thesis.

TABLE C.1

Basic Nuclear Data

BWR and PWR Problems

Material*	D_1 D_2	Σ_{a1} Σ_{a2}	$\nu\Sigma_{f1}$ $\nu\Sigma_{f2}$	Σ_{21} --
BWR Sample Problems				
A and B fuel	1.436+0 3.868-1	1.051-2 1.018-1	7.293-3 1.531-1	1.596-2 ---
A rod	1.092+0 3.507-1	3.185-3 4.021-1	0.0 0.0	0.0 ---
B rod and Water Reflector	1.545+0 3.126-1	4.440-4 8.736-3	0.0 0.0	2.838-2 ---
PWR Sample Problem**				
F_{12} Fuel	1.417+0 3.883-1	9.769-3 8.868-2	6.806-3 1.441-1	1.525-2 ---
F_{12} Shims	1.473+0 4.704-1	9.609-3 2.276-1	0.0 0.0	1.926-2 ---
E_{16} Fuel	1.420+0 3.891-1	9.512-3 8.109-2	6.277-3 1.278-1	1.558-2 ---

(continued on next page)

TABLE C.1 (continued)

Material*	D_1 / D_2	Σ_{a1} / Σ_{a2}	$\nu\Sigma_{f1}$ / $\nu\Sigma_{g2}$	Σ_{21} / --
E_{16} Shims	1.473+0	1.631-2	0.0	1.877-2
	4.662-1	2.951-2	0.0	---
D_0 and D_0^W Fuel	1.426+0	9.125-3	5.459-3	1.616-2
	3.903-1	6.917-2	1.021-1	---
Rod Channel (Water)	1.729+0	8.993-4	0.0	3.268-2
	2.914-1	1.582-2	0.0	---
Rod Channel (Control Rod)	1.208+0	7.017-2	0.0	1.481-2
	5.156-1	1.999-1	0.0	---
Shroud	8.617-1	3.442-3	0.0	5.124-3
	3.536-1	9.480-2	0.0	---
Water Reflector	1.817+0	7.495-4	0.0	3.585-2
	2.711-1	1.706-2	0.0	---

*Material notation for BWR problems refers to Fig. 2.1. PWR material notation refers to Fig. 3.4.

**The PWR two-strip problem includes assemblies F_{12} and E_{16}, the shroud, and the water reflector. The nuclear data for the remaining assemblies is listed for use in calculating albedoes and Cubic-Hermite expansions for various PWR assemblies (see Tables 3.2 and 3.3).

TABLE C.2

Boundary Albedoes for Sample Problems*

	BWR Reflector	PWR Reflector plus Shroud	PWR Albedoes for Side of Strip Opposite Reflector and Shroud
α_{11}	3.0806-1	5.1675-1	7.0000-1
α_{12}	0.0	0.0	0.0
α_{21}	1.4792-1	5.6037-2	0.0
α_{22}	7.8573-1	4.8802-1	5.0000-1

*Reflector albedoes are calculated using Kalambokas's[14] expressions. The albedoes listed in the last column were chosen to simulate possible reactor conditions.

TABLE C.3

Positional Albedoes for Sample Problems*

Assembly Position i	$[\alpha^1]_i$	$[\alpha^2]_i$	$[\alpha^3]_i$	$[\alpha^4]_i$
		BWR-Quarter Core		
Q1	B	wB	B	wB
Q2,Q4	A	wB	A	A
Q3,Q7	B	wB	B	B
Q5,Q9	B	B	B	B
Q6,Q8	A	A	A	A
		BWR-Half Core		
H1-H7,H9 are identical to Q1-Q7,Q9				
H8	B	A	A	A
H10	B	A	B	wB
H11	B	B	B	B
H12	B	A	B	B
H13	wB	B	B	wB
H14,H15	wB	B	B	B
		PWR Problem		
P1	E	wP	I	I
P2	Z	F	I	I

(continued on next page)

TABLE C.3 (continued)

*Assembly positions refer to Figures 4.1, 4.2 and 4.3. The assembly orientation used in the homogenization procedure is chosen such that the positional albedoes listed for each face ℓ, (see Figure 3.2), $[\alpha^{\ell}]_i$, are those of the surrounding material. The notation for each positional albedo matrix refers to the material albedo matrices listed in Tables 3.1, 3.2 and C.2 where A=albedo matrix of assembly A; B=albedo matrix of assembly B; wB=albedo matrix of the BWR water reflector; E=albedo matrix of assembly E_{16}; wP=albedo matrix of the PWR water reflector plus shroud; I=2 x 2 identity matrix; and Z=albedoes listed in third column of Table C.2.